International
Progress Report

IPR-00-29

Äspö Hard Rock Laboratory

TRUE Block Scale Project

Tracer test stage

Tracer tests, phase B

Peter Andersson
Eva Wass
Magnus Holmqvist
Geosigma AB

Thomas Fierz
Solexperts AG

December 2000

Svensk Kärnbränslehantering AB
Swedish Nuclear Fuel
and Waste Management Co
Box 5864
SE-102 40 Stockholm Sweden
Tel 08-459 84 00
+46 8 459 84 00
Fax 08-661 57 19
+46 8 661 57 19

Äspö Hard Rock
Laboratory

Report no.
IPR-00-29
No.
F56K
Author
Peter Andersson
Eva Wass
Magnus Holmqvist
Thomas Fierz
Date
Dec 2000
Checked by
Anders Winberg
Date
Feb 2001
Approved
Olle Olsson
Date
March 2001

Äspö Hard Rock Laboratory

TRUE Block Scale Project
Tracer test stage

Tracer tests, phase B

Peter Andersson
Eva Wass
Magnus Holmqvist

Geosigma AB

Thomas Fierz

Solexperts AG

December 2000

Keywords: TRUE, Block Scale, tracer tests, tracer dilution test,

This report concerns a study which was conducted for SKB. The conclusions and viewpoints presented in the report are those of the author(s) and do not necessarily coincide with those of the client.

Abstract

This report describes the performance and results of the second phase, Phase B, of the TRUE Block Scale Tracer Test Stage. Phase B included two series of tracer tests performed at different pump rates in the selected sink. In total ten tracer injections were performed in eight different flow paths of which two at different strengths of the sink. The tests were performed in both radially convergent and unequal dipole flow geometry. The main objectives of the tests were to increase the understanding of flow and transport in a fracture network and to serve as a basis for selecting suitable flow geometry for the planned tracer tests in Phase C of the project. This included use of dissolved Helium-3 gas which, in combined use with a conservative reference tracer, was used to study effects of matrix diffusion. Further, the tests in flow paths deemed suitable for tests with radioactive sorbing tracers were prolonged to demonstrate mass recovery of the non-sorbing species in excess of 80%. The tests produced a good quality data set where effects of different transport mechanisms such as diffusion are indicated. The results also served as an input to the final choice of tracer test geometry to be used for the planned tracer tests during Phase C of the project. At least three of the investigated flow paths were found to fulfil the requirements to be suitable for tracer tests with radioactive sorbing tracers.

Executive Summary

Presently the fourth and last of the defined stages of the TRUE Block Scale Project, the Tracer Test Stage, has started where the results of the performed characterisation is capitalised in the form of a series of tracer tests in the block scale (L=10-100 m). The second phase, Phase B, was performed with the main objective to investigate transport in fracture networks and to investigate heterogeneity within single fractures (structures #20 and #21). The tests also aimed to investigate the effects of fracture intersection zones (FIZ) and finally, to test the connectivity of the structures and mass recovery in order to select the best suitable geometry for the planned tracer test in Phase C of the Tracer Tests Stage.

The Phase B tests involved a total of ten different test set-ups, the three first (B-1a-c) with tracer injection in three different flow paths at a reduced withdrawal rate (Q=1.2 l/min) at the sink and the remaining seven tests (B-2a-g) with maximum withdrawal rate (Q=2.1 l/min) at the sink. All tests used the same sink section KI0023B:P6 which was selected based on results from Phase A (Andersson et al 2000). Two of the flow paths were also tested using Helium and a reference tracer to study diffusion effects.

The tracer injections were mostly performed by injecting with a constant flow throughout the entire duration of the test creating an uneven dipole flow field with injection flow rates in the order of 0.5-2% of the withdrawal rate. The main reason for using this technique was to increase the mass flux in the injection points and thereby also increase the possibility of detecting the tracer at the sink. Earlier tracer injections have preferably been performed in sections having high induced groundwater flow (measured by tracer dilution tests), while in Phase B most injection sections had low induced flow. This strategy turned out quite succesful as tracer breakthrough was measured from all ten injections made.

The Phase B tracer tests also included Helium (He-3) injections using equipment and techniques developed by SOLEXPERTS AG for the Grimsel tracer experiments (Frick et al, 1991). This equipment included in-line detection of Uranine in the injection and pumping sections as well as in-line detection of Helium in the pumping section. The Helium detection equipment worked well although it is rather sensitive to the ambient temperature at the site. This, in combination with breakthrough concentrations close to the background level made it necessary to correct for temperature effects. All other components of the injection and sampling systems worked well throughout the tests.

Four of the Phase B tests were performed with the objective to study diffusion effects making use of injection of Helium. The tests were performed in two different pathways, one "single" fracture path" (KI0025F03:P5) and one "network path" (KI0025F03:P6). The He and the reference tracer breakthrough curves show that Helium is delayed and has a more pronounced tailing than the reference tracer. The lower and delayed He peak indicates that diffusion as a transport process is more accentuated by the diffusive He. The longer tailing of the He breakthrough curve can also be explained by the more diffusive He.

It should be noted that the simple analysis made in this report can not be used as evidence that diffusion effects are actually observed. Not even the bad model fits obtained with the simple advection-dispersion model used in this report are evidence for such effects. A more thorough analysis, beyond the scope of this report is needed, where effects that may give similar results (e.g. heterogeneity, multiple flow paths) are considered. Another explanation for the difference may be effects of fracture intersection zones (FIZ) and this will be further analysed as a part of the TRUE Block Scale Evaluation and Reporting Stage (ERS).

The analysis and interpretation of the breakthrough curves reveal differences between the flow paths that indicate whether the transport occurs within a single fracture or within a network of fractures. The interpretation is generally consistent with the March ´00 structural model (Hermanson & Doe, 2000) but in two cases single fracture flow paths show breakthrough characteristics that indicate transport through a network of fractures. One of these paths is also interpreted to be close to a fracture intersection zone and one alternative explanation could be that transport occurs along this intersection having an enhanced pore volume and thus, decreasing the transport velocity. Another explanation may be that the involved structure (#21) is discontinuous or consists of several sub-parallel structures making up a much longer travel distance than the geometrical one.

The TRUE Block Scale Phase B tracer tests have involved a multitude of tracers in a multitude of different injection schemes within a relatively short time. The results of the tests were generally good, meaning that data of high quality could be produced for a number of different flow paths over distances between 15 to at least 100 meters. Given the results and conclusions presented in this report the general objective to "increase the understanding of transport in block scale" has been met although a complete understanding still is far away. The tracer retention aspect (through diffusion) has been enlightened by the use of Helium.

The tests have also provided input for selection of flow paths suitable for subsequent tests with sorbing tracers (Phase C). A recommendation (and possibly also a requirement) is to use flow paths with high tracer mass recovery. Based on the results presented in this report such flow paths are KI0025F03:P5, KI0025F03:P7 and KI0025F02:P3 (sink in KI0023B:P6).

Contents

1 Introduction

1.1 Background

The TRUE Block Scale project is an international partnership funded by ANDRA, ENRESA, Nirex, POSIVA, PNC and SKB (Winberg, 1997). The Block Scale project is one part of the Tracer Retention Understanding Experiments (TRUE) conducted at the Äspö Hard Rock Laboratory. The third of the defined experimental stages, the Detailed Characterisation Stage, has now been finalised (Winberg, 2000). Presently the final part in the experimental work, the Tracer Test Stage, is ongoing. Phase A of this stage including a large number of tracer dilution tests and two series of tracer tests in different flow regimes (tests A4 and A5) are being analysed and interpreted (Andersson et al., in prep.).

In Winberg, (2000) four basic questions are proposed for the planned tracer tests:

1. What is the conductive geometry of the TRUE Block Scale rock volume? Does the March 1999 structural model (and the results of the subsequent hydraulic reconciliation) reflects the conductive geometry with sufficient accuracy to allow design and perform tracer tests?

2. What are the properties of the fractures and fracture zones that control transport in networks of fractures?

3. How do the retention processes control transport in fracture networks, and how can they be measured in field tracer tests?

Hypotheses are proposed for each of these questions :

H1) **"The major conducting structures of the target volume for tracer tests in the TRUE Block Scale rock volume trend north-west and are subvertical. Being subvertical, and subparallel, they do not form a conductive network in the designated target volume. For the purpose of testing fracture network flow and transport effects in the current borehole array, second-order NNW features are required to provide the necessary connectivity between the major conducting NW structures!"**

H2a) **"Fracture intersections have distinctive properties and have a measurable influence on transport in fracture/feature networks. These distinctive properties may make the intersection a preferential conductor, a barrier, or a combination of both!"**

H2b) **"In-plane heterogeneity and anisotropy have a measurable influence on transport of solutes in a block scale fracture network!"**

H3) **"It is not possible to discriminate between breakthrough curves of sorbing tracers in a single fracture from those obtained in a network of fractures"!**

1.2 Objectives

The primary objective of the Tracer Test Stage is to provide the data from which we can "increase understanding, and the ability to predict" "transport in a fracture network" in the block scale, i.e. over a length scale of 10-100 m. In addition, to "assess the importance of tracer retention mechanisms (diffusion and sorption) in a fracture network" (Winberg, 2000).

The specific objectives for the Phase B tracer tests are:

- To investigate transport in fracture networks
- To investigate heterogeneity within single fractures (structures #20 and #21)
- To investigate the effects of fracture intersection zones (FIZ)
- To revisit earlier investigated flow paths and verify high mass recovery. This will serve as input for selection of flow paths for sorbing tracer tests (Phase C)

The specific objective for each tracer test and the coupling to the hypotheses are presented in Table 1-1.

Table 1-1. Objectives and hypotheses addressed with Phase B tracer tests B1 and B2. The structural interpretation and notation refers to the updated March 2000 model, cf. Figure 1-1 (Hermanson & Doe, in prep.)

Test* #	Flow path	Structures	Objective	Hypotheses tested
B-1a	KI0025F03:P5 – KI0023B:P6	20, 21	Helium diffusion, FIZ effects, heterogeneity of structure #20	2, 3
B-1b	KI0025F03:P6 – KI0023B:P6	22, 20, 21	Diffusion without Helium (comparison with B-2a)	3
B-1c	KI0025F02:P5 – KI0023B:P6	20, 21	Test of new flow path and heterogeneity within structure #20	1, 2
B-2a	KI0025F03:P6 - KI0023B:P6	22, 20, 21	Effect of pump rate on Helium diffusion, network effects	2, 3
B-2b	KI0025F02:P3 - KI0023B:P6	21	Heterogeneity within structure #21, Phase C preparation	1, 2
B-2c	KA2563A:S1 – KI0023B:P6	19, 13, 21	Network transport	1, 2
B-2d	KI0025F03:P7 – KI0023B:P6	23, 20, 21	Network transport	1, 2
B-2e	KI0025F03:P3 – KI0023B:P6	21	Heterogeneity within structure #21, FIZ effects	1, 2
B-2g	KI0025F03:P5 - KI0023B:P6	20, 21	Phase C preparation. Only needed if B-1a shows significant mass losses	2
B-2h	KI0025F02:P6 - KI0023B:P6	22, 20, 21	Phase C preparation. Check of mass recovery. Comparisons with test PT-4.	-

* Test B-2f cancelled and replaced by B-2h

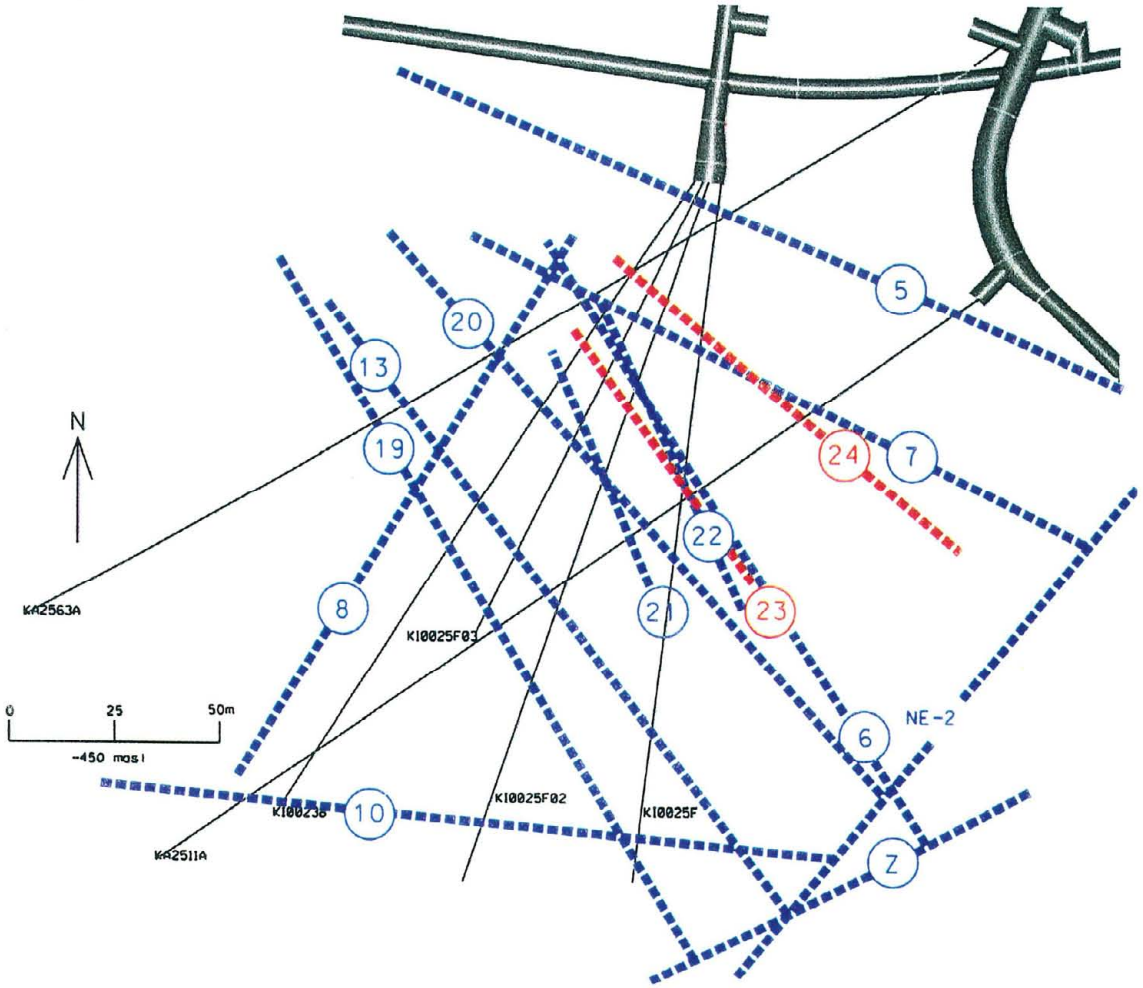

Figure 1-1. Schematic view of the March 2000 hydro-structural model (Hermanson & Doe, in prep.)

2 Performance and evaluation procedure

2.1 Equipment and tracers used

Each of the four characterisation boreholes involved in the tests is instrumented with 6-10 inflatable packers isolating 5-10 borehole sections. Each borehole section is connected to a pressure transducer which is connected the Äspö hydro monitoring system (HMS). Each of the sections used for tracer tests are equipped with three nylon hoses, two with an inner diameter of 4 mm and one with an inner diameter of 2 mm. The two 4-mm hoses are used for injection, sampling and circulation in the borehole section whereas the 2-mm hose is used for pressure monitoring.

The tracer tests were performed using five identical equipment set-ups for tracer tests, i.e. allowing five sections to be measured simultaneously. A schematic drawing of the tracer test equipment is shown in Figure 2-1. The basic idea is to have an internal circulation in the borehole section. The circulation makes it possible to obtain a homogeneous tracer concentration in the borehole section and to sample the tracer concentration outside the borehole in order to monitor the injection rate of the tracer with time.

Circulation is controlled by a pump with variable speed (A) and measured by a flow meter (B). In sections with low flow rates, the tracer will be forced into the flow path by applying a slight excess pressure using an external water injection pump (unequal strength dipole flow geometry). Water and tracer injections are made with two different HPLC plunger pumps (C1 and C2) and sampling is made by continuously extracting a small volume of water from the system through a flow controller (constant leak) to a fractional sampler (D). Water for injection is stored in a pressurised vessel (E1) under nitrogen atmosphere. The tracer solution was injected from a 1-litre plastic bottle that was placed on a scale. An optional tracer storage vessel is also available (E2) but was not used in Phase B. The tracer test equipment has earlier been used in the TRUE-1 tracer tests (e.g. Andersson, 1996).

For the tests including Helium (He-3) special equipment was applied by SOLEXPERTS AG, described in section 2.2.

The tracers used were four fluorescent dye tracers, Uranine (Sodium Fluorescein) from KEBO (purum quality), Amino G Acid from Aldrich (technical quality), Rhodamine WT from Holiday Dyes Inc. (technical quality) and Naphtionate from Fluka (purum quality). These tracers have all been used previously in the TRUE-1 tracer tests (Winberg et al., 2000) and in the TRUE Block Scale Pre-tests (Andersson et al., 1999) and Phase A tests (Andersson et al., 2000). In addition, a number of metal complexes (m-EDTA and DTPA) were used. The metals were synthesised at Dep. of Nuclear Chemistry, CTH, Gothenburg using metal salts from Aldrich (>99.9 % purity) and DTPA and EDTA-complexes from Sigma (>99 % purity). The chosen metals are

presented in Table 2-2. The metal complexes were also spiked with an Amino-G Acid solution to enable a better and less expensive control of the source term in each section.

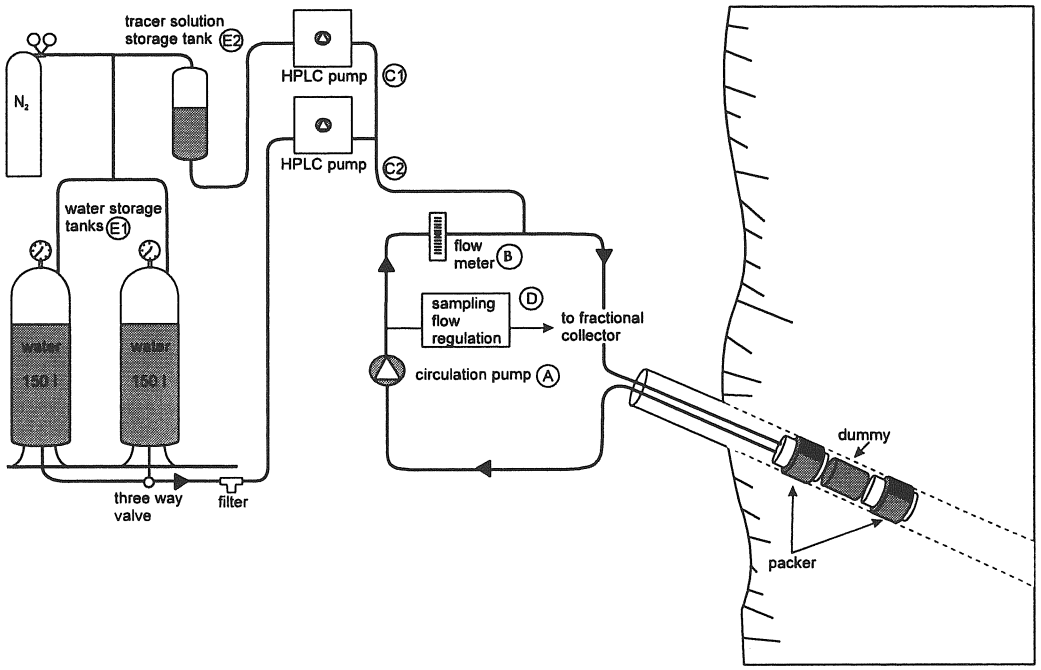

Figure 2-1. Schematic drawing of the tracer injection/sampling system used in the TRUE Project.

2.2 Equipment for Helium tests

2.2.1 Injection side

In order to create a dipole flow field, non-traced groundwater was stored in a water reservoir. The injection flow of the dipole flow field was established using an HPLC pump (Shimadzu LC8). The reservoir water passed through a filter to prevent small particles from causing malfunction of the injection pump. Before being fed into the injection interval, the water passed a flow meter, which determined the injection flow rate. The set up is shown in Figure 2-2 and the equipment components are listed in Table 2-1.

Table 2-1. Dipole injection equipment

Equipment component
Dipole injection pump (Shimadzu LC8, range: 0.1 – 150 ml/min)
Filter (mesh width 0.4 microns)
Flow meter (Fisher and Porter, inductive)
Tracer tank (stainless steel, volume ca 3 litre)
Balance (Mettler, resolution: 0.1 g)
Flow-through cell for Uranine detection (fittings 6mm Swagelok T-piece)
Stainless steel lines (od 6 mm) for circulation circuit including tracer inlet port and bypass for fluorescence flow-through cell
Water reservoir with sufficient volume (min. 50 litres)
Nitrogen including pressure regulating valve with 6mm Swagelok fitting
Circulation pump

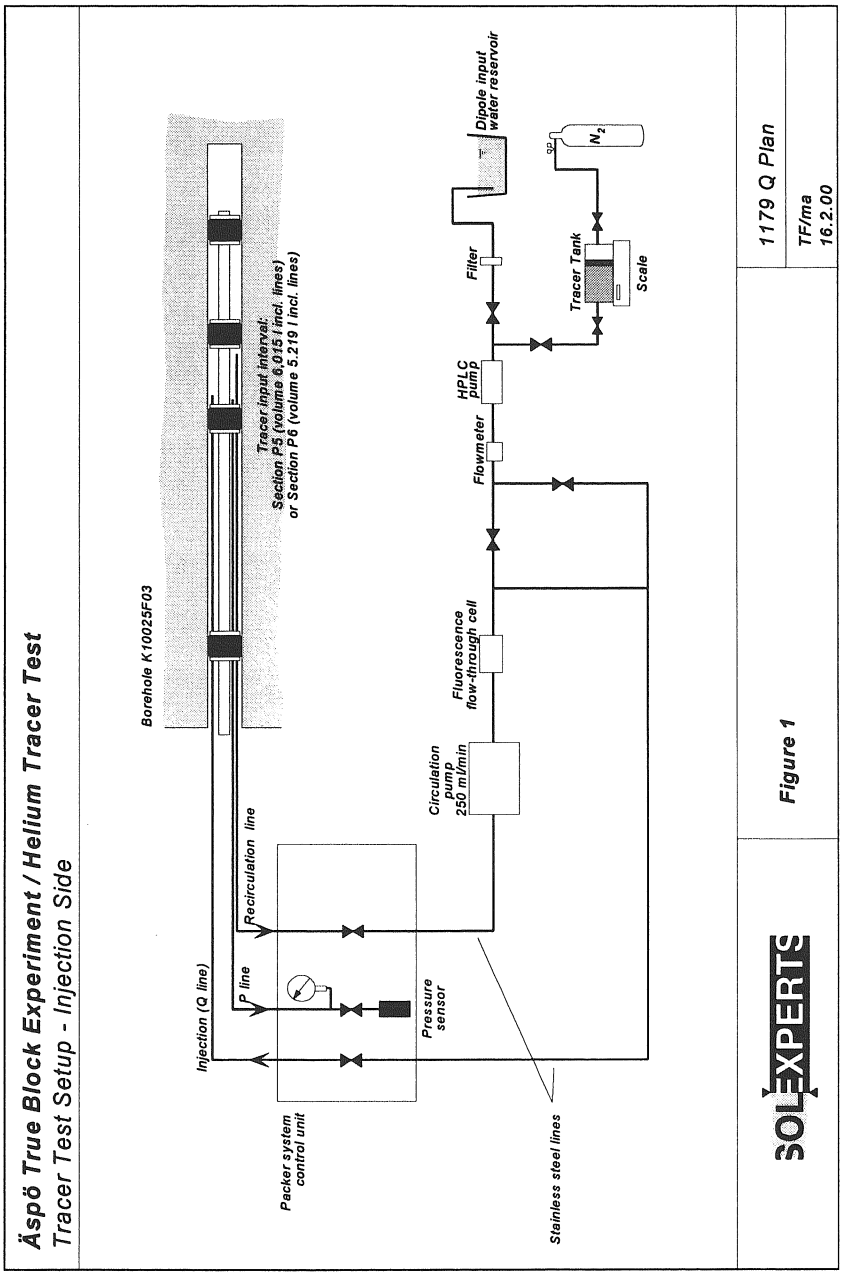

Figure 2-2. Equipment at the injection side.

2.2.2 Extraction side

The extraction side instrumentation is shown in Figure 2-3. In order to obtain in-line He concentration measurements, the standard extraction set-up was in addition equipped with the following components:

- Inlet port for calibration
- Bypass for He flow through-cell

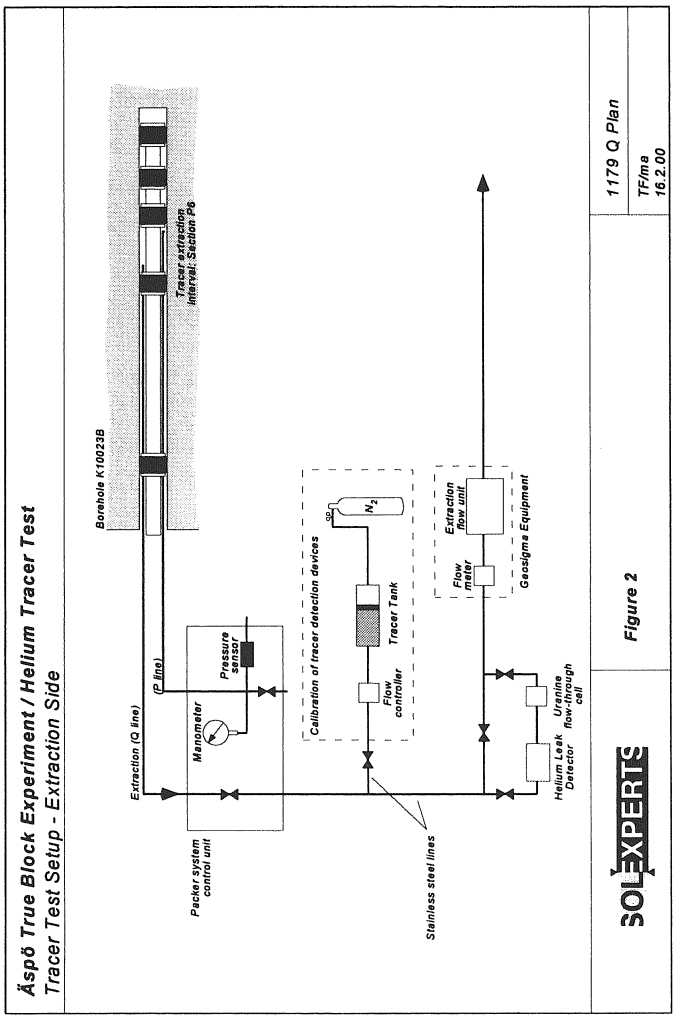

Figure 2-3. Equipment at the extraction side.

2.3 Performance of the Phase B tracer tests (B-1, B-2)

Tracer test Phase B was divided in two sub-phases, B-1 and B-2. Sub-phase B-1 was performed in three selected flow paths (cf. Table 2-2) using a reduced pump flow rate (about 50 % of maximum possible) in the selected sink section KI0023B:P6 (including structure #21). The idea was to increase the possibility to observe diffusive processes. Sub-phase B-2 involved seven flow paths using maximum possible pump flow rate in KI0023B:P6. The dimension of the tubing and the transmissivity of the section then only restricted the flow.

Table 2-2. Performance of Phase B tracer tests. The structural interpretation and notation refers to the March 2000 model (Hermanson & Doe, in prep.). Distances within brackets are calculated along the structures.

Test #	Flow path	Struc -tures	Flow geometry	Inj. Flow (ml/min)	Pump flow (ml/min)	Tracer	Distance
B-1a	KI0025F03:P5 – KI0023B:P6	20,21	Dipole	45	1200	Helium, Uranine	14 (16)
B-1b	KI0025F03:P6 – KI0023B:P6	22,20 ,21	Dipole	20	1200	Amino G	15 (73)
B-1c	KI0025F02:P5 – KI0023B:P6	20,21	Dipole	10	1200	RdWT	21 (21)
B-2a	KI0025F03:P6 – KI0023B:P6	22,20 ,21	Dipole	20	2060	Helium, (Uranine), Yb-EDTA	15 (73)
B-2b	KI0025F02:P3 – KI0023B:P6	21	Rad Conv	1.6	2060	$NaReO_4$	33 (33)
B-2c	KA2563A:S1 – KI0023B:P6	19,13 ,21	Rad Conv	0.5	2060	Ho-DTPA	55 (>)
B-2d	KI0025F03:P7 – KI0023B:P6	23,20 ,21	Dipole	10	2060	Gd-DTPA	17 (97)
B-2e	KI0025F03:P3 – KI0023B:P6	21	Dipole	10	2060	In-EDTA	27 (27)
B-2g	KI0025F03:P5 – KI0023B:P6	20,21	Dipole	45	2060	Helium, (Uranine), Naphtionate	14 (16)
B-2h	KI0025F02:P6 – KI0023B:P6	22,20 ,21	Rad Conv	12.7	2060	Rhodamine WT	18 (65)

The flow geometry was radially converging in flow paths with high flow rates (q> 30 ml/h) according to Phase A tracer dilution tests (Andersson et al, 2000) and tracer dilution tests performed in the Pre-tests (Andersson et al., 1999). In sections with low flow rates, the tracer was forced into the flow path by applying a slight excess pressure using an external water injection pump (dipole).

The water used for injection during B-1 and B-2 was extracted from borehole section KA3385A:P1 which has a very similar water chemistry to the target structures in the TRUE Block Scale array. The water from KA3385A:P1 was led through nylon tubing directly into two, nitrogen filled, pressurised (5-6 bars) stainless steel storage vessels.

The flow data from the sink section was stored on a field logger (Borre 21) during the pumping with reduced flow rate. The flow from the pumped section together with the electrical conductivity of the pumped water was also measured manually during the pumping period.

The positions of the sink and source sections used for tracer injections in the TRUE Block Scale Phase B tests B-1 and B-2 are shown in Figure 2-4.

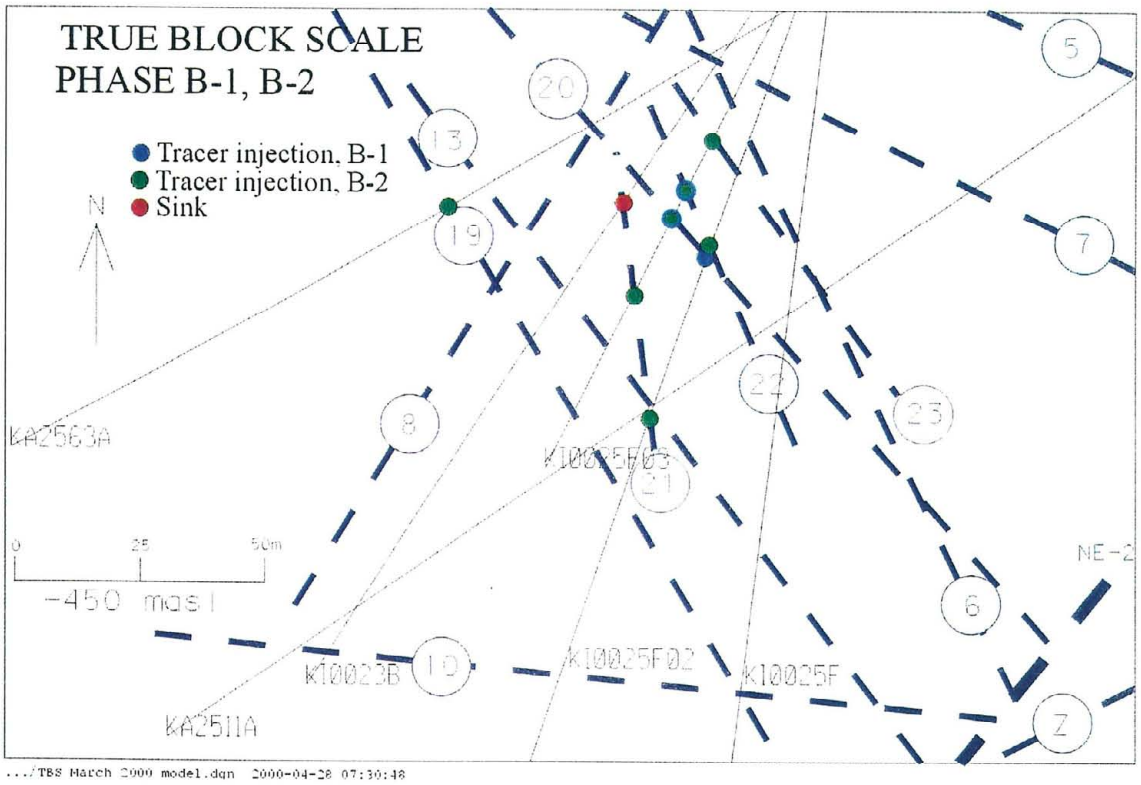

Figure 2-4. Positions of sink, dilution test sections and tracer injection (source) sections during the TRUE Block Scale Phase B tests B-1 and B-2. The positions of the structures are based on the March 2000 structural model (Hermanson & Doe, in prep.). Z=-450 masl.

2.4 Tracer detection

2.4.1 Laboratory analyses

Samples were analysed for dye tracer content at the GEOSIGMA Laboratory, Uppsala, using a Jasco FP777 Spectrofluorometer. The metal complexes were analysed at SGAB Laboratory, Luleå using ICP/MS.

2.4.2 Helium detection technique

The concept of on-line He detection is based on a flow-through cell with two chambers separated by a highly gas-permeable membrane. The fluid passes through one chamber. In the second chamber, the He leak tester creates a vacuum. The dissolved gases in the fluid are extracted through the gas-permeable membrane into the vacuum chamber, which is connected to the mass spectrometer of the He leak tester (Figure 2-5). The He concentration in the fluid is proportional to the leak rate through the membrane as long as the fluid flow rate and the pressure are constant. The leak rate of the tracer input solution must be determined prior to the tracer tests by a calibration run. Both the He input and the breakthrough concentrations are measured as leak rates [mbar liter/sec]. For a relative and M_0-normalized (M_0: tracer input mass) breakthrough curve, conversion to absolute concentrations is not required [ccHe(STP)/ml].

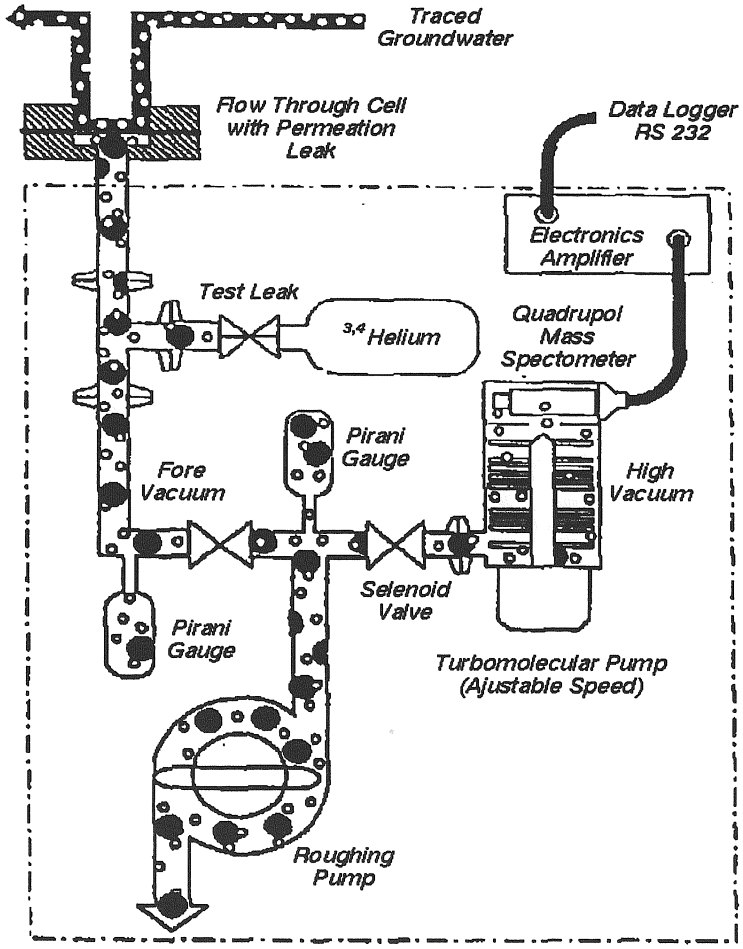

Figure 2-5. Schematic illustration of He detection technique.

On-line detection of Uranine

Uranine is measured in flow-through cells using a fiber optic fluorometer. One flow-through cell is installed into the injection interval circuit (monitoring of tracer dilution within the injection interval circuit). The second cell is integrated into the pumping flow line (due to the high Uranine background of the pumping water, Uranine could not be used for breakthrough monitoring). An Argon laser (blue light 488 nm) is utilized as light source. A beam splitter divides the laser beam; hence two optical quartz fibers can be connected to the light source. The emitted light of the fluorescent tracer is transferred by a second optical quartz fiber to the analysis device, which is equipped with a high voltage power supply, an amplifier and two photomultipliers. The photomultiplier signal caused by the emitted light is proportional to the tracer concentration. The device was developed and manufactured by SOLEXPERTS and has been routinely used for several years at the GTS Migration experiment (Frick et al., 1992).

2.5 Evaluation

2.5.1 Tracer dilution tests

Flow rates were calculated from the decay of tracer concentration versus time through dilution with natural unlabelled groundwater, c.f. Winberg (*ed*), (1996). The so-called "dilution curves" were plotted as the natural logarithm of concentration versus time. Theoretically, a straight-line relationship exists between the natural logarithm of the relative tracer concentration (c/c_0) and time (t):

$$Q_{bh} = -V \cdot \Delta \ln (c/c_0) / \Delta t \qquad 2\text{-}1$$

where Q_{bh} (m^3/s) is the groundwater flow rate through the borehole section and V (m^3) is the volume of the borehole section.

2.5.2 Tracer test

The evaluation of the tracer test has involved computer modelling using a simple one-dimensional advection-dispersion model (Van Genuchten & Alves, 1982). From the computer modelling, dispersivity and mean travel times were determined using an automated parameter estimation program, PAREST (Nordqvist, 1994). PAREST uses a non-linear least squares regression where regression statistics (correlation, standard errors and correlation between parameters) also is obtained.

The chosen one-dimensional model assumes a constant fluid velocity and negligible transverse dispersion, cf. Equation 2-2.

$$\partial C/\partial t = D(\partial^2 C/\partial x^2) - v \cdot \partial C/\partial x \qquad 2\text{-}2$$

where: D = Dispersion coefficient
v = fluid velocity (m/s)
C = concentration of solute
x = distance from injection point (m)
t = time (s)

According to Ogata & Banks (1961) and Zuber (1974), the dispersion in a radially converging flow field can be calculated with good approximation by equations valid for one-dimensional flow. Although a linear flow model (constant velocity) is used for a converging flow field, it can be demonstrated that breakthrough curves and parameter estimates are similar for Peclet numbers of about 10 and higher.

Van Genuchten (1982) gives a solution for step input with dispersion over the injection boundary. The solution of Equation 2-2, then is:

$$C/C_o = \tfrac{1}{2}\,\mathrm{erfc}\,[(x-v\cdot t)/Z] + (V/\pi)^{1/2} \exp\,[(x-v\cdot t)^2/(4D\cdot t)] - \tfrac{1}{2}\,[1+v\cdot x/D+V] \exp\,[v\cdot x/D]\,\mathrm{erfc}[(x+v\cdot t)/Z] \qquad 2\text{-}3$$

where: $Z = 2(D\cdot t)^{1/2}$

$V = v^2 t/D$

Variable injection schemes were simulated by superposition of the solution given in Equation 2-3.

The fit of the breakthrough curves using a three-parameter fit included velocity, v, dispersion coefficient, D, and the so called F-factor which corresponds to injected mass divided by fracture volume, M_{inj}/V_f. The result of the evaluation is presented in Chapter 3.3.2 and 3.4.3.

Based on the mean travel times, t_m, determined from the parameter estimation, the hydraulic fracture conductivity, K_{fr} (m/s), were calculated assuming radial flow and validity of Darcy's law (Gustafsson & Klockars, 1981);

$$K_{fr} = \ln (r/r_w)\,(r^2-r_w^2)/2\cdot t_m\cdot\Delta h \qquad 2\text{-}4$$

where: r = travel distance (m)
r_w= borehole radius (m)
t_m= mean travel time of tracer (s)
Δh= head difference (m)

The equivalent fracture aperture, b (m), was calculated from:

$$b = Q \cdot t_m / \pi \cdot (r^2 - r_w^2) \qquad 2\text{-}5$$

where Q (m^3/s), is the mean pumping rate.

Flow porosity, θ_k, was calculated using:

$$\theta_k = K / K_{fr} \qquad 2\text{-}6$$

where K is the hydraulic conductivity of the packed-off section of the borehole determined from steady state evaluation of the interference test (Moye, 1967):

$$K = (Q / \Delta h \cdot L) \cdot ((1 + \ln L / 2r_w) / 2\pi) \qquad 2\text{-}7$$

where L (m) is the length of the packed-off section. It should be noted that the term flow porosity might be misleading to use in a fractured heterogeneous rock as it is defined for a porous media. However, it is often used in fractured media as a scaling factor for transport, but then defined over a finite thickness which, in his case, is defined as the length of the packed-off borehole section (L = 1.0 m).

The values calculated using Equations 2-4 through 2-7 are presented together with parameters determined from the numerical modelling of the tracer breakthrough in Table 3-6 (B-1) and Table 3-11 (B-2).

Tracer mass recovery was calculated in two different ways. Common for both methods is that the tracer mass recovered in the pumping borehole is determined by integration of the breakthrough curves for mass flux (mg/h) versus time (h). The injected mass is determined in the same way but also by weighing the tracer solution vessel during the injection procedure.

3 Results and interpretation

3.1 General

The performance of the B-1 and B-2 tests was somewhat affected by problems with the water injection pumps used for creating the dipole flow. The time sequence for injection and all problems related to the tests are listed in the Log of Events (Table 3-1). A serious experimental problem also occurred when tracer breakthrough of Uranine from a previous injection during Phase A (A-5) in KI0025F02:P3 was detected. This breakthrough had a very long tailing and concealed the breakthrough of the Uranine injected together with He in test B-1a. Hence, in test B-2a one metal-complex, Yb-EDTA, was also injected together with He and Uranine to provide the necessary conservative reference, cf. Table 2-2. In the third test containing He, test B-2g, a dye tracer, Naphtionate, was used as a reference tracer. Test B-2f was cancelled since Yb-EDTA was used in test B-2a instead. An additional test, B-2h, was performed to check the mass recovery for the flow path KI0025F02:P6 - KI0023B:P6, since the mass recovery in test B-2a was low.

3.2 Log of events

Table 3-1. Log of events (borehole notations are shortened by removing the prefix "KI00-" from the borehole labels.

Date	Event
	Test B-1 (Q_{pump}=1200 ml/min)
000309	Start tracer dilution tests, F02:P5, F03:P5, F03:P6, no pumping
000310	Start pumping KI0023B:P6. Q=1200 ml/min. Flow regulation unstable. Manual regulation. Pumping decreased gradually to Q=950 ml/min (000313)
000313	Increased pumping rate in 23B:P6, Q=1200 ml/min. Stop tracer dilution tests.
000314	Installation of automatic flow regulation
000315	Testing pressure responses as a result of different water injection rates in sections F03:P6, F03:P5 and F02:P5.
000320	Start injection of water for dipole in F02:P5 and F03:P6
000321	Start tracer injection in F03:P6 (Amino-G Acid), test B-1b, and in F02:P5 (RdWT), test B-1c.

Date	Event
000325	Reduced capacity of dipole injection in F03:P6 due to clogging of filter
000327	Stop water injection in F03:P6, change of filter, re-start water injection in F03:P6
000327	Stop injection of water in F02:P5 and F03:P6 due to power failure
000328	Re-start water injection in F02:P5 and F03:P6, reduced flow (clogging of filter)
000328	Stop water injection in F02:P5 and F03:P6, change of filter, re-start water injection in F02:P5 and F03:P6
000328	Start injection of water for dipole in F03:P5 (SOLEXPERTS)
000328	Start tracer injection in F03:P5 (Helium, Uranine), test B-1a
000328	Stop injection of water in F03:P5, pump failure
000329	Re-start water injection in F03:P5
000403	Stop water injection in F03:P6
000406	Stop water injection in F02:P5
000406	Increased pumping in 23B:P6, Q=2090 ml/min
000414	Stop water injection in 25F03:P5
	Test B-2 (Q_{pump}=2100 ml/min)
000418	Removed flow regulator in 23B:P6, Q increased to 2100 ml/min
000425	Start injection of water for dipole in F03:P3 and F03:P7, Q=10 ml/min
000426	Start tracer injection in F03:P3 (In-EDTA), test B-2e, F03:P7 (Gd-DTPA), test B-2d, F02:P3 ($NaReO_4$), test B-2b and KA2563A:S1 (Ho-DTPA), test B-2c
000502	Power failure (15 minutes)
000502	Start injection of water for dipole in F03:P6, Q=20 ml/min
000503	Start tracer injection in F03:P6 (Helium, Yb-EDTA), test B-2a
000505	Reduced capacity of dipole injection in F03:P6 due to pump failure
000508	Injection capacity in F03:P6 back to normal
000522	Stop injection of water in F03:P6
000522	Start injection of water for dipole in F03:P5, Q=45 ml/min

Date	Event
000522	Start tracer injection in F03:P5 (Helium, Naphtionate), test B-2g
000523	Start tracer injection in F02:P6 (Rhodamine WT), test B-2h
000523	Stop injection of water in F03:P7, pump failure
000524	Re-start injection of water in F03:P7
000529	Stop injection of water in F03:P5, pump failure
000530	Stop injection of water in F03:P3
000606	Stop injection of water in F03:P7
000614	Start Phase C
000908	Last sample taken for Phase B

3.3 Test B-1

3.3.1 Dilution tests

Test B-1 included measurements of flow rates using the tracer dilution method in the three sections selected to be injection sections in the tracer test. The tests were performed both under natural gradient and during pumping (reduced flow rate, 1200 ml/min) by flowing section KI0023B:P6 (structure #21) in order to study the influence of the pumping. During the 78-hour flow period the flow rate was decreased from 1.20 l/min to 0.95 l/min. The flow was manually regulated due to an equipment failure with the automatic flow regulator prior to the start. After necessary repair the flow regulator was installed after the performance of the dilution tests.

All three sections show a clear influence of the pumping in KI0023B:P6 with a flow increase of a factor 2-3 due to the pumping, Table 3-2. The dilution curves presented as the logarithm of concentration (Ln C) versus time are shown in Figure 3-1.

Table 3-2. Results of tracer dilution tests during test B-1 using KI0023B:P6 (#21) as sink.

Test section	Structure	$Q_{natural}$ (ml/h)	Q_{pump} (ml/h)	ΔQ (ml/h)
KI0025F02:P5	20	21	47	+ 26
KI0025F03:P5	20	7	15	+ 8
KI0025F03:P6	22	54	176	+ 122

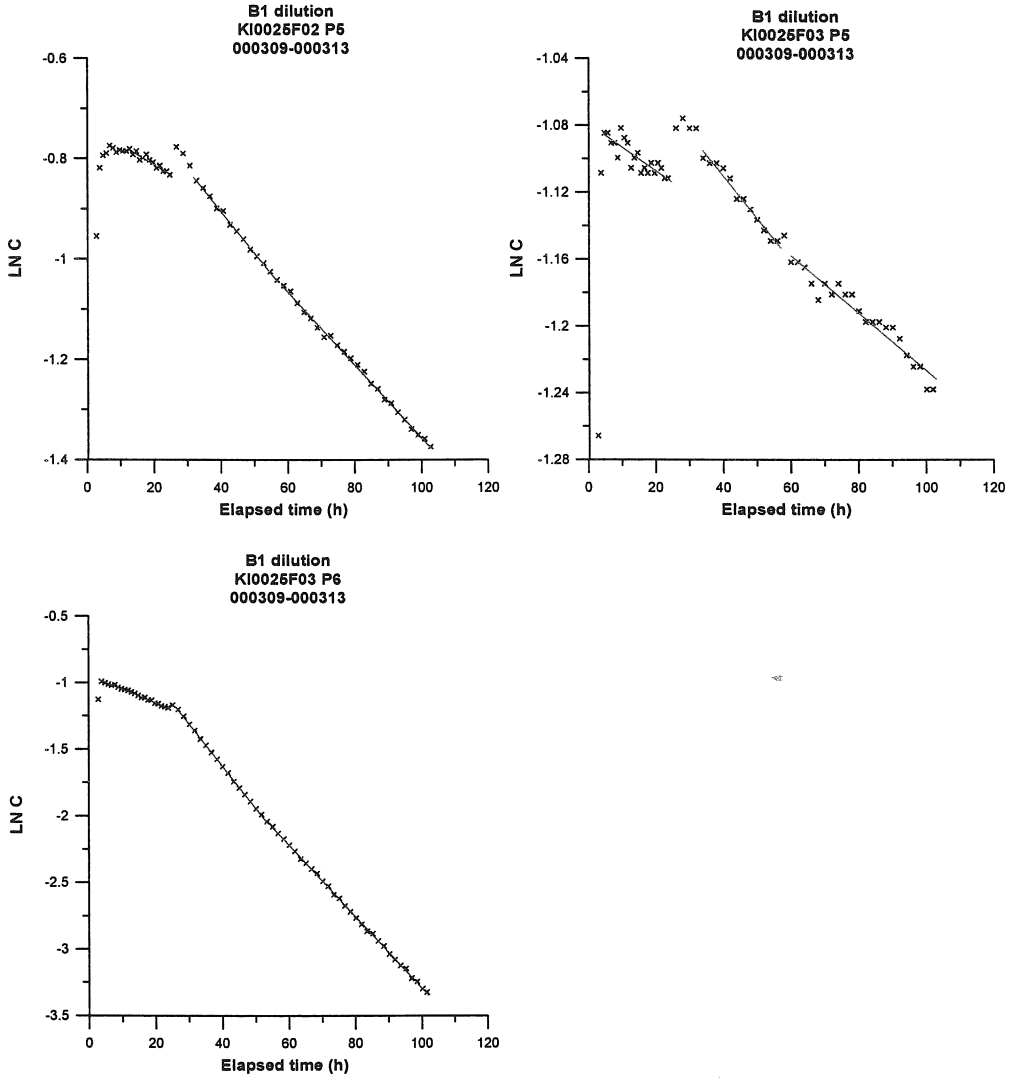

Figure 3-1. Tracer dilution curves (Ln C versus time) including straight-line fits for the borehole sections KI0025F02:P5, KI0025F03:P5 and KI0025F03:P6 in test B-1, before and after pump start in KI0023B:P6. Note that the axis scales differ.

3.3.2 Tracer tests

Test B-1 also involved unequal strength dipole tracer tests, using KI0023B:P6 as sink. Three sections were selected for injections, KI0025F02:P5, KI0025F03:P5 and KI0025F03:P6. Pumping was done in KI0023B:P6 (structure #21) using a reduced flow, 1.2 l/min, i.e. about 50 % of the maximum possible.

Tracer injections

All three tracer tests in B-1 (B-1a-c) were performed in an unequal strength dipole flow geometry. The injection concentrations and injection rates are given in Table 3-3 and are the actually measured ones.

Table 3-3. Tracer injection data for test B-1 (measured values).

Test #	Inj. Section	Structure #	Tracer	Max inj. conc (mg/l)	Inj rate (ml/min)*	Inj mass (mg)	Section Volume (ml)
B-1a	KI0025F03:P5	20, 21	Helium	-	-	-	7214
			Uranine	1.24	40	12.5[2]	
B-1b	KI0025F03:P6	22, 20, 21	Amino-G Acid	1266	11.2	8719[1] 11287[2]	5687
B-1c	KI0025F02:P5	20, 21	Rhodamine WT	976	8.0	5305[1] 6054[2]	6110

*= Calculated from the tracer dilution during injection
[1]= calculated by integration
[2]= calculated by weighing

The injection functions for test B-1a, B-1b and B-1c presented as the logarithm of concentration (Ln C) versus time are shown in Figure 3-2. The input function for test B-1a is also shown in Figure 3-3.

The injection rates calculated from the injection functions gives for all injections lower flow rates compared to the values set on the injection pumps. The expected flow rates were for B-1a 45 ml/min, for B-1b 20 ml/min and for B-1c 10 ml/min. All three tests used different injection pumps and a flow meter was only used in test B-1a. The difference between the flow meter value and the tracer dilution value may be explained by the fact that the flow meter shows too high values. This is also indicated by the fact that a similar difference shows up in test B-2 (cf, Section 3.4.1). In tests B-1b and B-1c no flow meter was used but it is likely that the pump capacity is somewhat lower than the pre-set value due to the high injection pressure (>40 bars). Thus, for all calculations flow values based on tracer dilution have been used.

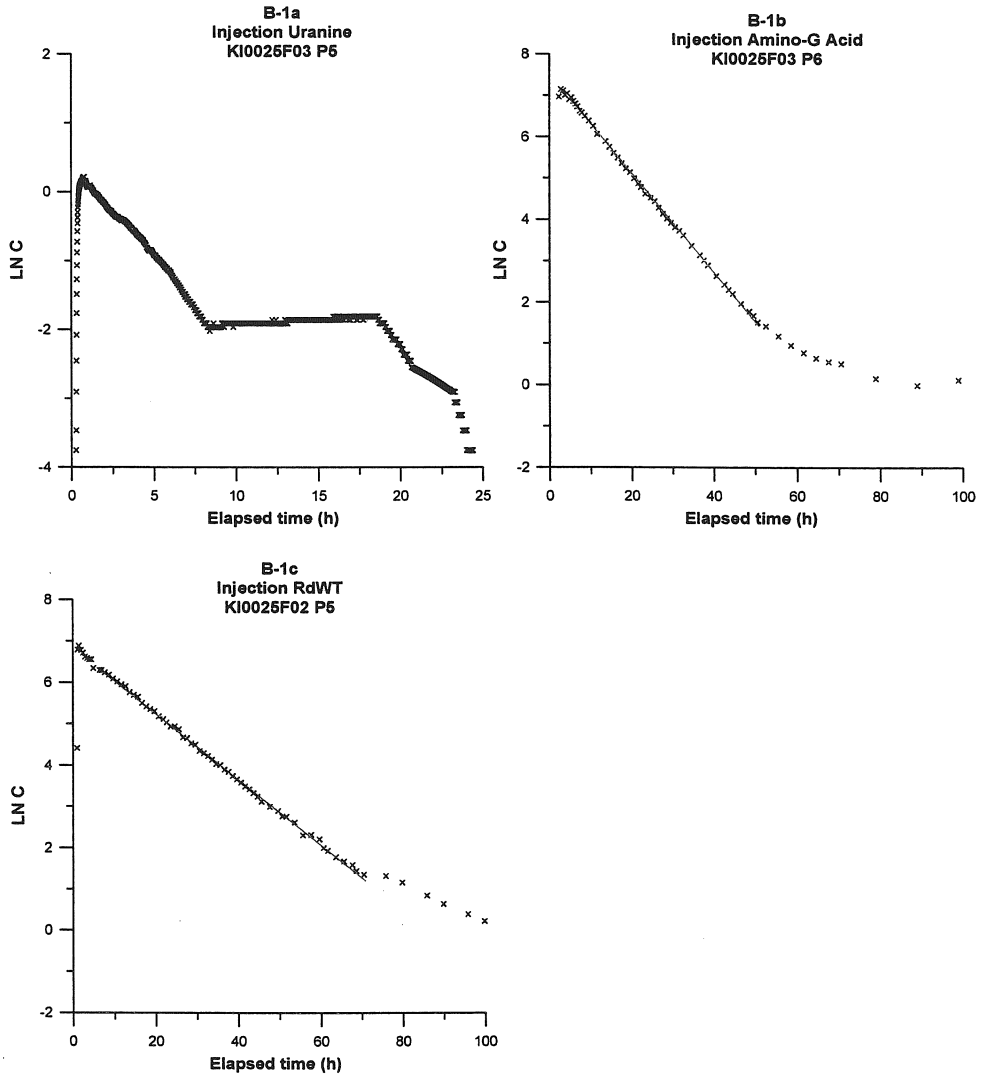

Figure 3-2. Tracer injection functions (Ln C versus time) including straight-line fits for the three injections during test B-1. Note that the axis scales differ.

Helium test B-1a

The tracer input function, represented in Figure 3-3, shows the concentration normalised by the tracer input mass. The cumulative curve represents the amount of tracer that has been injected at a given time. Tracer dosage was performed over 28 min with 45 ml/min (same flow rate as dipole injection flow rate). During tracer dosage the dipole injection flow was stopped. Prior to the tracer dosage, circulation through the injection interval was started with a flow rate of about 200 ml/min. The dipole injection pump failed 8 hours after the tracer dosage after about 90% of the tracer had been injected into the formation (see Figure 3-3). The remaining 10% of the tracer were injected after restart of the dipole injection pump.

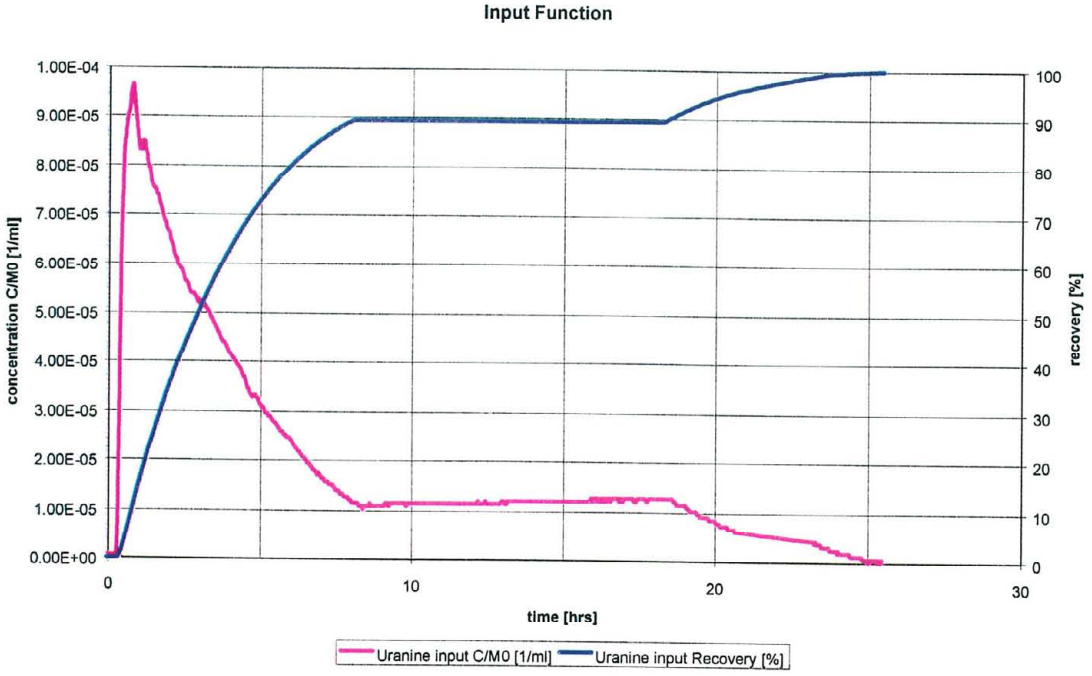

Figure 3-3. Tracer input function. From 8–16 hours after tracer dosage, the dipole injection pump failed. During this period, no diffusion within the interval fluid was observed. Therefore, no tracer input was assumed during the period with no dipole inflow.

Tracer breakthrough

Tracer breakthrough was detected in the sink section KI0023B:P6 from all three injections and the resulting breakthrough curves are presented in Figure 3-4 through 3-6. The breakthrough and injection curves for test B-1b and B-1c are also co-plotted (as mass flux versus time, log-log) in Appendix 1.

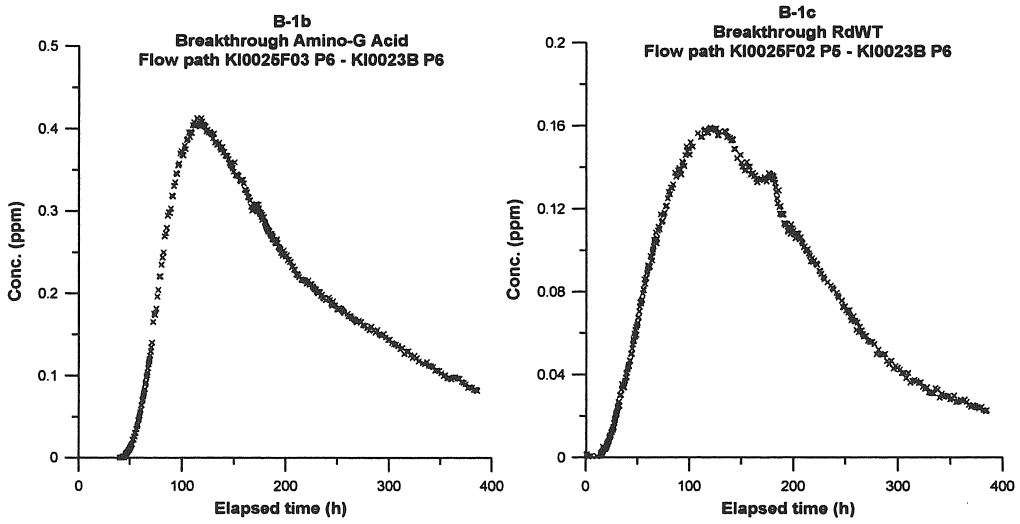

Figure 3-4. Tracer breakthrough in KI0023B:P6 during tests B-1. Note that the axis scales differ between the plots.

Tracer mass recovery for Amino-G Acid and Rhodamine WT was calculated in two different ways. Common to both methods is that the tracer mass recovered in the pumping borehole is determined by integration of the breakthrough curves for mass flux (mg/h) versus time (h). The injected mass is determined in the same way but also by weighing the tracer solution vessel during the injection procedure. The injected masses are shown in Table 3-3.

The mass recovery for Amino-G Acid and Rhodamine WT calculated from integration is higher than the recovery calculated by weighing (Table 3-4). The reason for this is further discussed in Section 3.4.2. The end of the tail of the breakthrough curves still remains to be recovered, and it is therefore likely that the mass recovery would have increased by another 5-10 % had the test been prolonged.

Table 3-4. Tracer mass recovery from pumping section KI0023B:P6 during test B-1.

Test #	Inj. Section	Structure	Tracer	R_i (%)	R_w (%)	Sampling time (h)
B-1a	KI0025F03:P5	20, 21	Helium	-	100	332
			Uranine	-	-	-
B-1b	KI0025F03:P6	22, 20, 21	Amino-G Acid	59	46	386
B-1c	KI0025F02:P5	20, 21	Rhodamine WT	42	37	385

R_i=recovery calculated by integration
R_w=recovery calculated by weighing

Helium test B-1a

The flow field KI0025F03:P5 –> KI0023B:P6 revealed a complete tracer breakthrough with 100% tracer recovery. A complete He-3 breakthrough was monitored, but Uranine detection (reference tracer) failed. Therefore, no comparison between Helium and a less diffusive tracer as Uranine is possible.

Table 3-5. Results test B-1a.

	He-3	Reference tracer *
First arrival [hrs]	6.7	-
Peak [hrs]	32.5	-
Peak C/Mo [1/ml]	$2.37\ 10^{-7}$	-
Ratio $peak_{He}$ / $peak_{reftracer}$	-	-
Tracer recovery measured [%]	100 %	-
Tracer recovery extrapolated [%]	100 %	-
Duration of tracer input function [hrs]	25.5	-

* = no results due to high background of Uranine

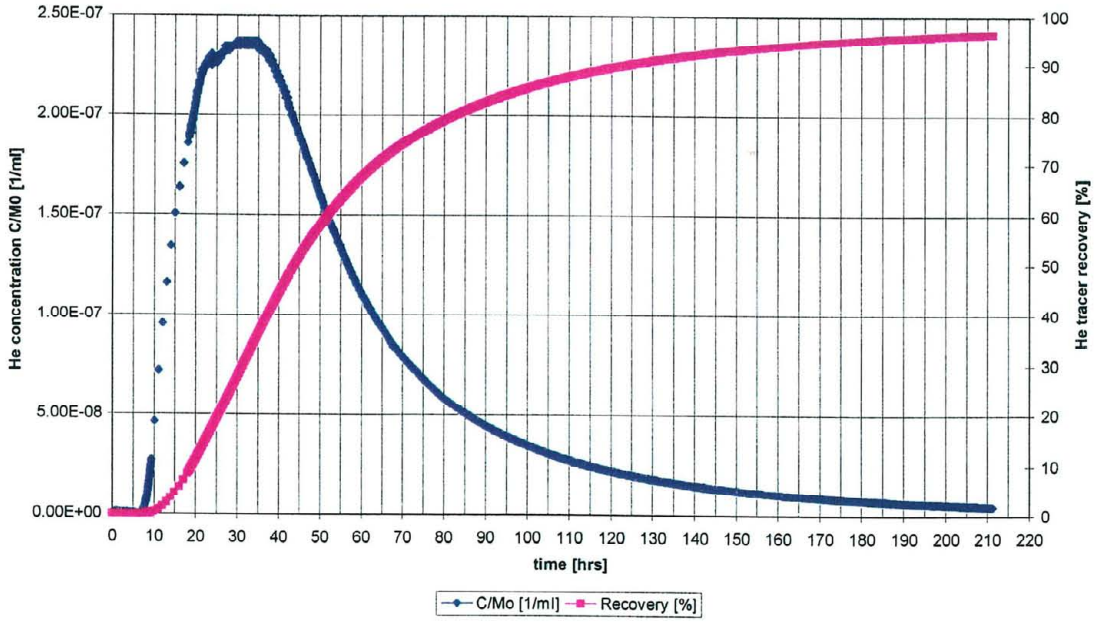

Figure 3-5. Run B-1a; He-3 breakthrough curve. Concentrations are normalised by the input mass(linear scales).

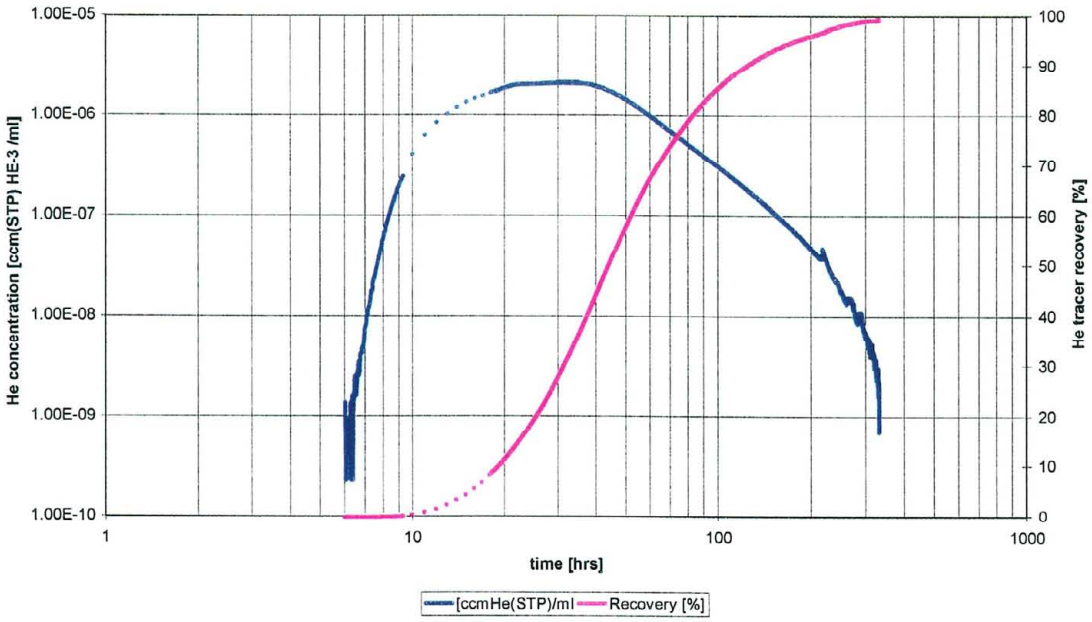

Figure 3-6. Run B-1a; He-3 breakthrough curve, absolute He-3 concentrations (logarithmic scales).

Numerical modelling and analytical interpretation

The breakthrough curves from two of the injections (KI0025F02:P5 and KI0025F03:P6) in test B-1 were evaluated using the one-dimensional advection-dispersion model described in Section 2.5.2.

The transport parameters derived from the numerical modelling and the analytical expressions described in Section 2.5.2 are presented in Table 3-6.

The best-fit runs for each tracer/flow path are presented in Figure 3-7. The modelling resulted in fits with low standard errors, 1-2 %. The breakthrough curve for Rhodamine WT (KI0025F02:P5 – KI0023B:P6) was quite well fitted while the curve for Amino-G Acid (KI0025F03:P6 – KI0023B:P6) was somewhat worse. The modelling results indicate that the description of the transport paths is more complicated than the simple approach used.

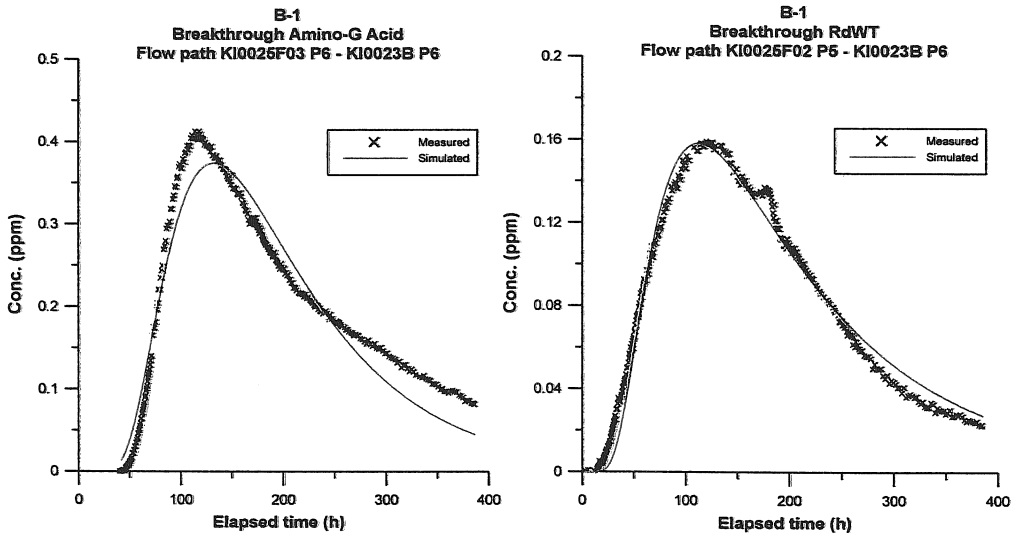

Figure 3-7. Comparison between measured and simulated tracer breakthrough in KI0023B:P6 during test B-1, cf. Table 3-6 for evaluated parameters. Note that the axis scales differ between the plots.

Table 3-6. Summary of hydraulic and transport parameters for the flow paths tested in B-1 using KI0023B:P6 as sink. Values within brackets are standard errors in percent.

Parameter	B-1b KI0025F03:P6	B-1c KI0025F02:P5	Source
Distance along fractures (m)	73	21	Geometry
Euclidean distance, L (m)	15	21	Geometry
Mean head difference, Δh (m)	89.1	77.1	HMS
Inj. flow rate (ml/min)	11	8	Injection curve (see Table 3-3)
Mean velocity, v (m/s)	$2.60 \cdot 10^{-5}$ (1)	$3.81 \cdot 10^{-5}$ (1)	PAREST
Mean travel time, t_m (h)	160.1 (1)	153.0 (1)	PAREST
First arrival, t_a (h)	46	15.5	Breakthrough curve
Dispersivity, D/v (m)	2.4 (2)	6.2 (2)	PAREST
Peclet number, Pe	6.1	3.4	PAREST
Fracture conductivity, K_{fr} (m/s)	$1.3 \cdot 10^{-5}$	$3.3 \cdot 10^{-5}$	Eq. 2-4
Equivalent fracture aperture, b (m)	$1.6 \cdot 10^{-2}$	$8.0 \cdot 10^{-3}$	Eq. 2-5
Flow porosity (1 m thickness)	$9.9 \cdot 10^{-3}$	$3.9 \cdot 10^{-3}$	Eq. 2-6
Mass recovery, R (%)	>59 >46*	>42 >37*	Breakthrough curve

*=recovery calculated by weighing

3.4 Test B-2

Test B-2 involved tracer injections in seven different sections, using KI0023B:P6 as sink. Four tests were performed in an unequal strength dipole flow geometry while three were radially converging tracer tests, cf Table 2-2. Pumping was done in KI0023B:P6 (structure #21) using maximum possible flow, Q=2.1 l/min.

3.4.1 Tracer injections

Four of the tracer tests in B-2 (B-2a, d, e and g) were performed in a dipole flow geometry, while three tests (B-2b, c and h) were performed as radially converging tracer tests. The injection concentrations and injection rates are given in Table 3-7 and are the actually measured ones. The metal complexes were also spiked with an Amino-G Acid solution to enable an improved and less expensive control of the source term in each section. Due to a greater number of data points, the injection rate determined from Amino-G Acid in each section was also used for calculations of mass flux and recovery for the corresponding metal complex.

Table 3-7. Tracer injection data for test B-2 (measured values).

Test #	Inj. Section	Structure #	Tracer	Max inj. Conc (mg/l)	Inj rate (ml/min)*	Inj mass (mg)	Section Volume (ml)
B-2a	KI0025F03:P6	22, 20, 21	Helium	-	-	-	5687
			Uranine	0.92	11.8	11.93[2]	
			Yb-EDTA	278	11.9	2243[1]	
						3749[2]	
B-2b	KI0025F02:P3	21	ReO_4	378	1.59	2917[1]	8424
						3738[2]	
B-2c	KA2563A:S1	19, 13, 21	Ho-DTPA	580	0.50	3872[1]	9081
						5834[2]	
B-2d	KI0025F03:P7	23, 20, 21	Gd-DTPA	337	8.4	2323[1]	4978
						3003[2]	
B-2e	KI0025F03:P3	21	In-EDTA	269	9.6	2404[1]	6287
						2815[2]	
B-2g	KI0025F03:P5	20, 21	Helium	-	-	-	7214
			Uranine	0.65	38	3.73[2]	
			Naphtionate	218	34	2204[1]	
						2674[2]	
B-2h	KI0025F02:P6	22, 20, 21	Rhodamine WT	339	12.7	3408[1]	9916
						2937[2]	

* = Calculated from the tracer dilution during injection
[1] = calculated by integration
[2] = calculated by weighing

The injection functions presented as the logarithm of concentration (Ln C) versus time are shown in Figures 3-8 and 3-9. The figures show that the dilution of Amino G Acid and the corresponding metal complexes are very similar which indicates that no sorption of the complexes occur on the borehole walls. The calculated flow rates for Amino G Acid and the metal complexes are within ± 10% for all injections.

Also during test B-2 the calculated injection rates were lower than the flow rates given by the flow meter. The expected flow rates were for B-2a 20 ml/min (12 ml/min from dilution), for B-2d and 2e 10 ml/min (8.4 and 9.6 from dilution) and for B-2g 45 ml/min (34 ml/min from dilution). The difference between the flow meter values and the tracer dilution values is rather large for test B-2a and B-2g and the most likely explanation is that the flow meter (which was the same in both tests and in test B-1a) shows too high values. This is also indicated by the fact that three different tracers show the same flow rate from dilution in test B-2a. In tests B-2d and B-2e no flow meter was used but it is likely that the pump capacity is somewhat lower than the pre-set value due to the high injection pressure (>40 bars).

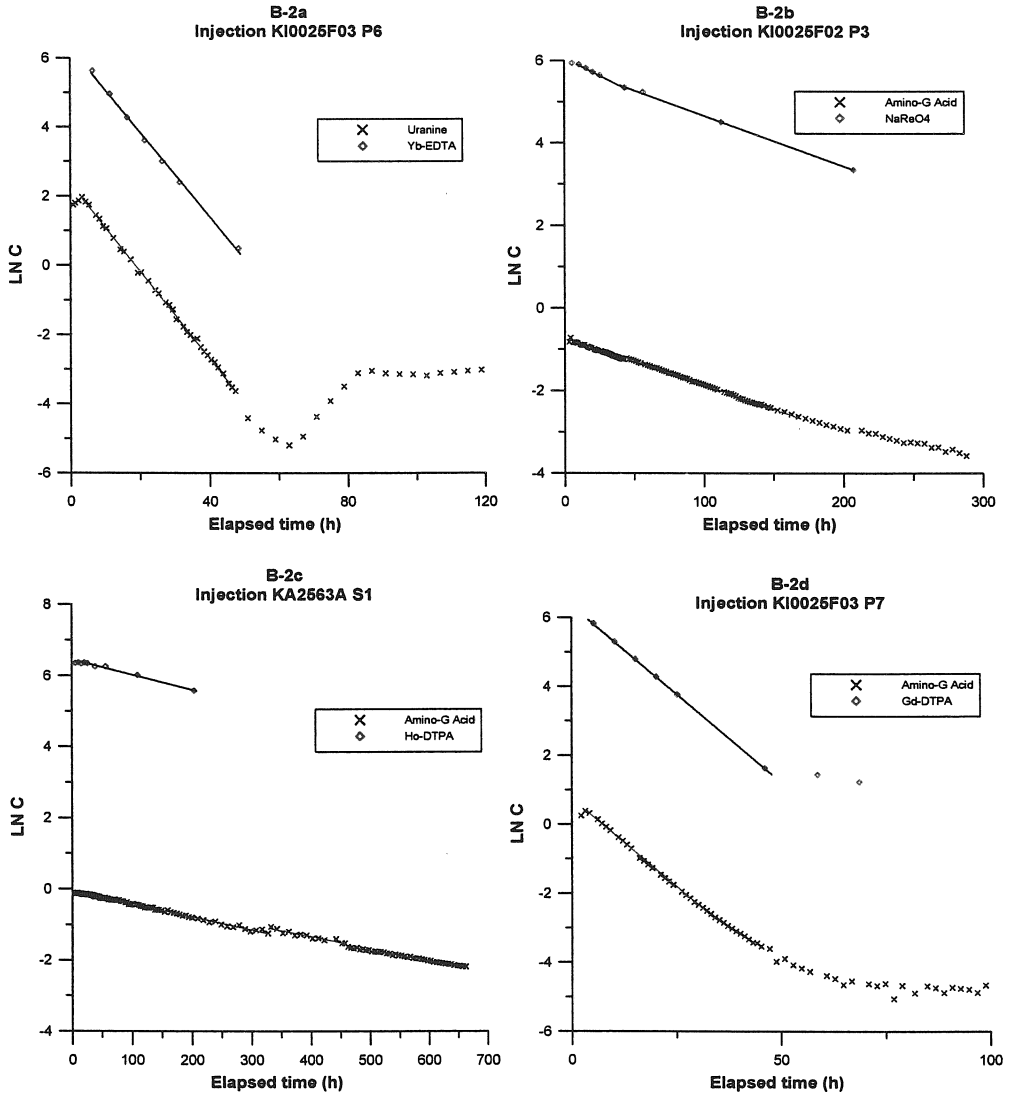

Figure 3-8. Tracer injection functions (Ln C versus time) including straight-line fits for the injections during test B-2a - B-2d. Note that the axis scales differ.

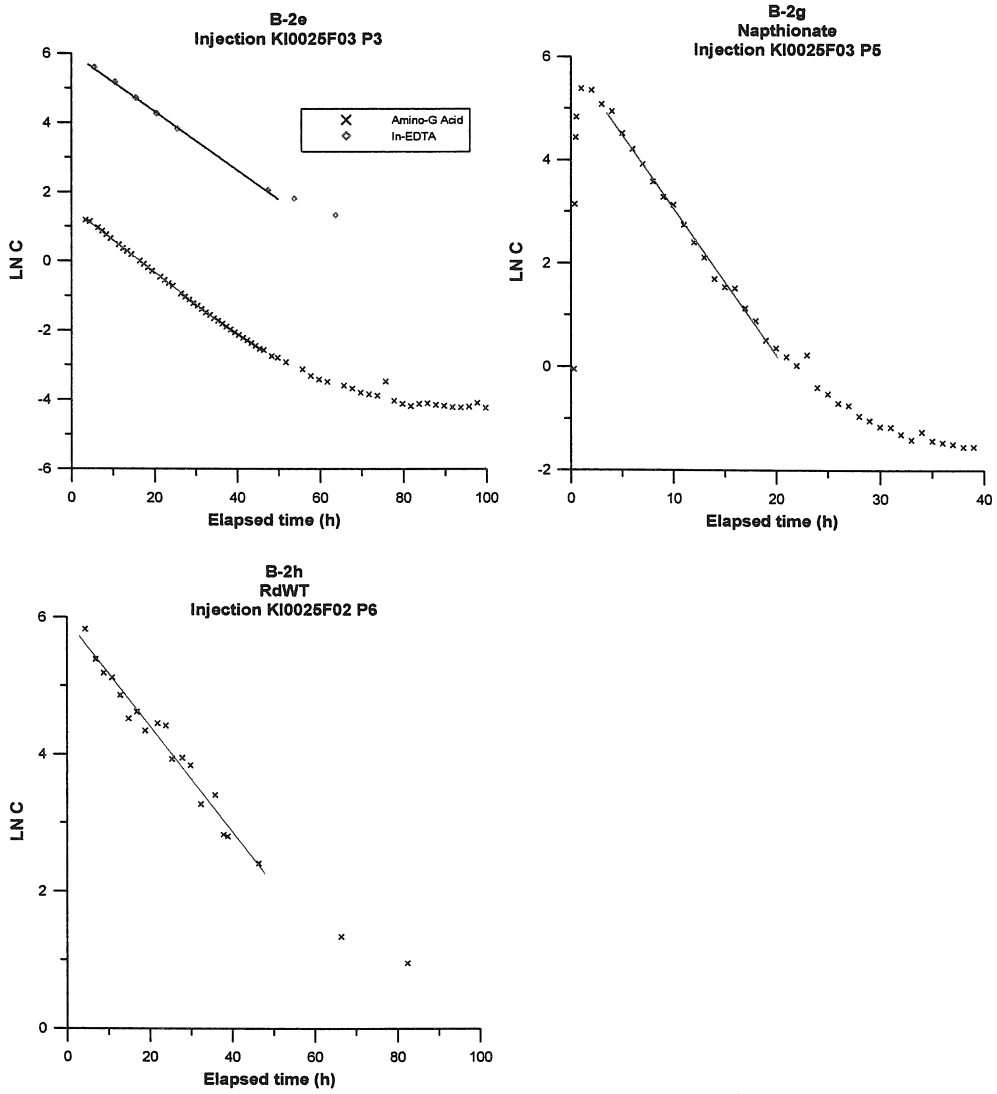

Figure 3-9. Tracer injection functions (Ln C versus time) including straight-line fits for the injections during test B-2e – B-2h. Note that the axis scales differ.

Helium test B-2a

The tracer input function, represented in Figure 3-10, shows the concentration normalised by the tracer input mass. The cumulative curve represents the amount of tracer that was injected at a given time after the start of the tracer dosage. Tracer dosage was performed during 52 min. Two injection pumps were used, one for the Helium/Uranine solution with a dosage rate of 28.3 ml/min and second pump for the Yb-EDTA tracer solution with a dosage rate of 10 ml/min. To keep the dipole injection rate (20 ml/min) constant, 18 ml/min was extracted out of the back flow line of the injection interval circuit during the dosage period. Prior to the tracer dosage, circulation through the injection interval was started with a flow rate of about 110 ml/min.

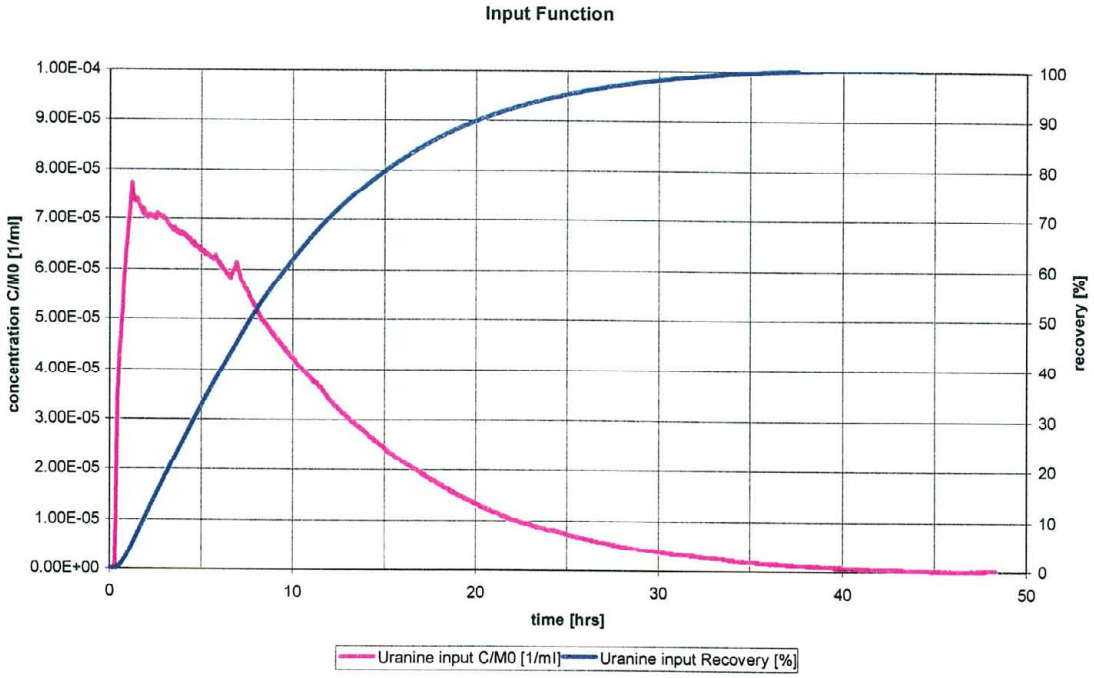

Figure 3-10 Run B-2a;Tracer input function. Concentrations are normalised by the input mass Mo; it is assumed that the Uranine input function is also valid for Helium (He-3) and Yb-EDTA, which were injected simultaneously.

Helium test B-2g

The tracer input function, represented in Figure 3-11, shows the concentration normalised by the tracer input mass. The recovery curve represents the amount of tracer that was injected at a given time after the start of the tracer dosage. Tracer dosage was performed over 10 min for the He-3/Uranine solution and over 28 min for the Naphtionate solution. Two injection pumps were used, one for the He Uranine solution with a dosage rate of 35 ml/min, and a second pump for the Naphtionate tracer solution with a dosage rate of 10 ml/min. Prior to the tracer dosage, circulation through the injection interval was started with a flow rate of about 215 ml/min.

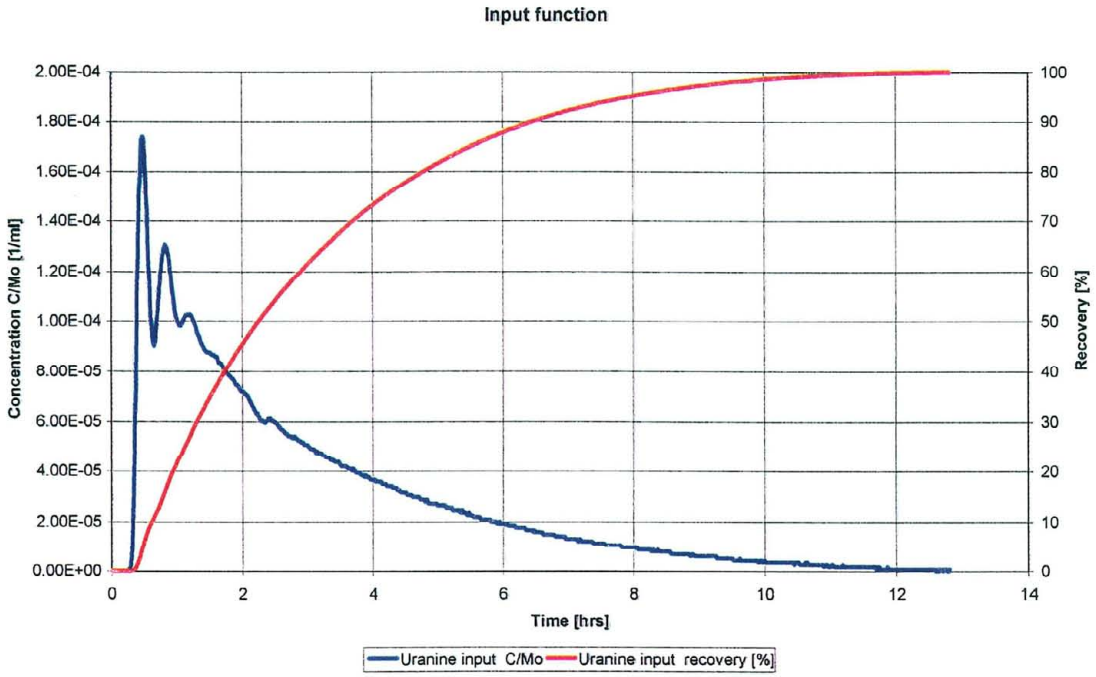

Figure 3-11 Run B-2g; Tracer input function. Concentrations are normalised by the input mass Mo; it is assumed that the Uranine input function is only valid for Helium (He-3). Naphtionate tracer dosage started simultaneously but lasted 18 min longer than the He dosage.

3.4.2 Tracer breakthrough

The breakthrough of tracer was monitored in the sink section KI0023B:P6. Tracer breakthrough was detected from all seven injections performed and the resulting breakthrough curves are presented in Figure 3-12. The breakthrough and injection curves (except for He) are also co-plotted (as mass flux versus time, log-log) in Appendix 1.

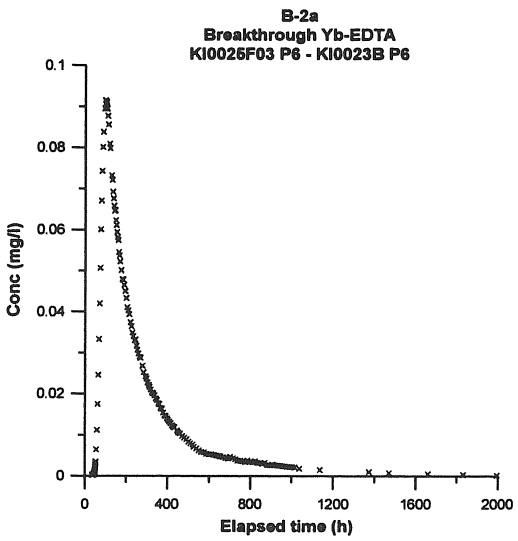
B-2a
Breakthrough Yb-EDTA
KI0025F03 P6 - KI0023B P6
Conc (mg/l)
Elapsed time (h)

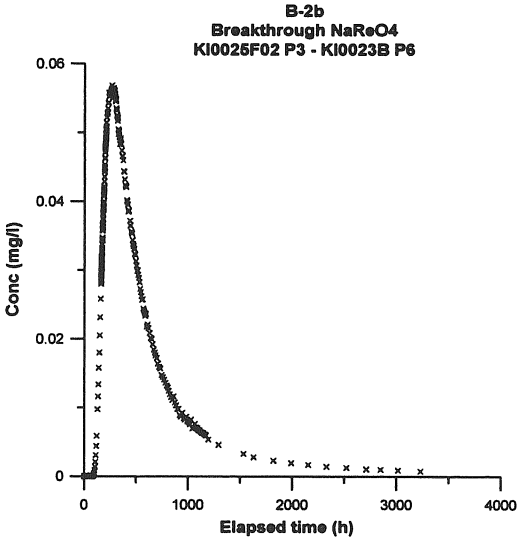
B-2b
Breakthrough NaReO4
KI0025F02 P3 - KI0023B P6
Conc (mg/l)
Elapsed time (h)

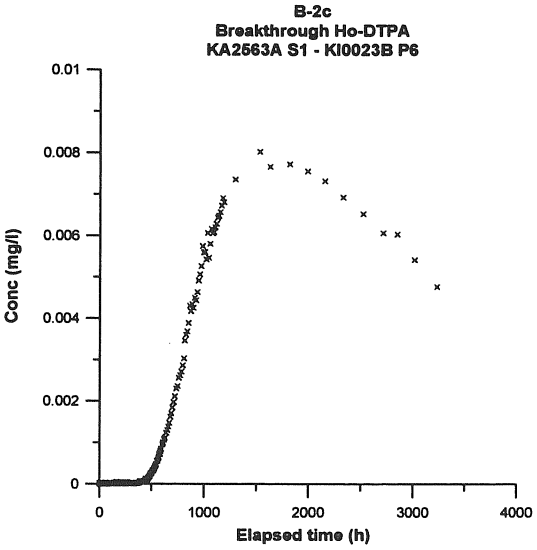
B-2c
Breakthrough Ho-DTPA
KA2563A S1 - KI0023B P6
Conc (mg/l)
Elapsed time (h)

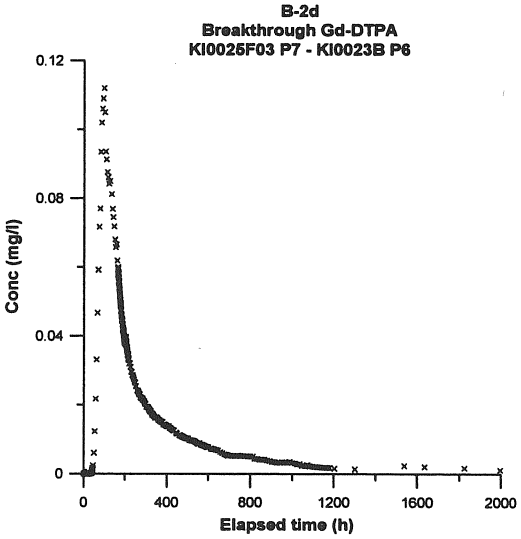
B-2d
Breakthrough Gd-DTPA
KI0025F03 P7 - KI0023B P6
Conc (mg/l)
Elapsed time (h)

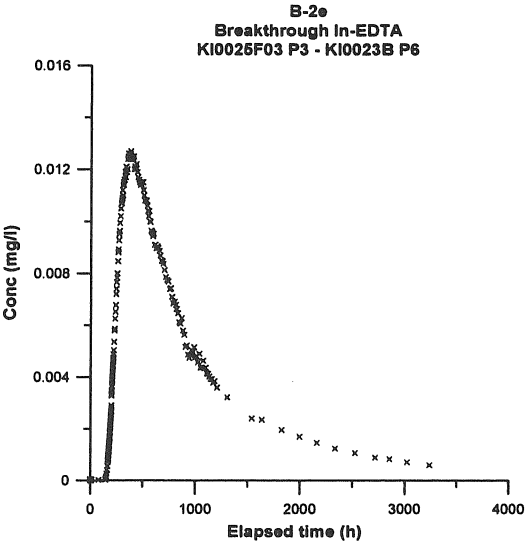
B-2e
Breakthrough In-EDTA
KI0025F03 P3 - KI0023B P6
Conc (mg/l)
Elapsed time (h)

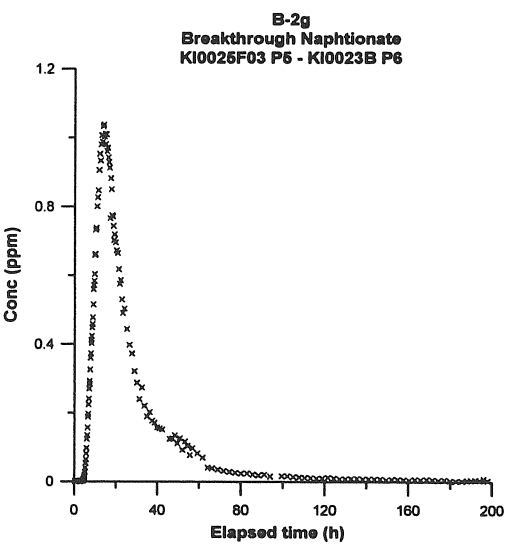
B-2g
Breakthrough Naphtionate
KI0025F03 P5 - KI0023B P6
Conc (ppm)
Elapsed time (h)

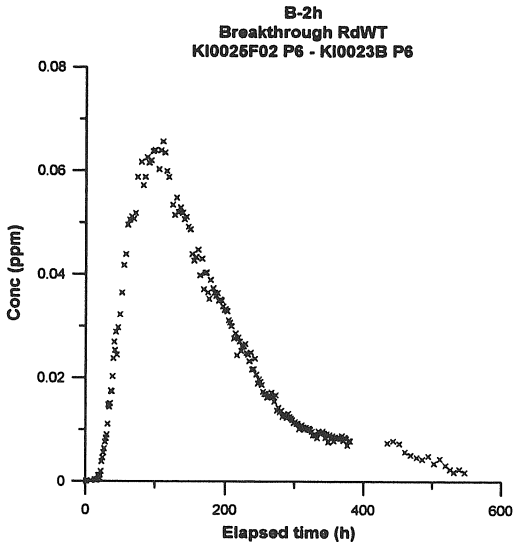

Figure 3-12. Tracer breakthrough in KI0023B:P6 during test B-2. Note that the axis scales differ between the plots.

The pumping continued as Phase C was started and samples for test B-2 were taken once a week after start of Phase C, cf. Section 3.2.

Tracer mass recovery was calculated in two different ways. Common for both methods is that the tracer mass recovered in the pumping borehole is determined by integration of the breakthrough curves for mass flux (mg/h) versus time (h). The injected mass is determined in the same way but also by weighing the tracer solution vessel during the injection procedure. The calculated injected masses, both integrated and weighed, are shown in Table 3-7.

The mass recovery calculated from integration was constantly higher than the recovery calculated by weighing (Table 3-8), except for Rhodamine WT. In some cases the recovery calculated from integration was >100 %, which is totally unrealistic. One explanation for this may be that a larger volume is injected in the section (5-10 ml/min) than what is possible to withdraw with the sampling equipment (q_{max}=1.67 ml/min). This creates an overpressure and tracer solution is pushed into the fracture and is never accounted for in the samples and in the concentration measurements. The injected mass determined by integration is then underestimated resulting in too high figures of the mass recovery.

Calculations of the tracer mass recovery (Table 3-8) show high mass recovery for Naphtionate injected in KI0025F03:P5, ReO_4 injected in KI0025F02:P3 and Gd-DTPA injected in KI0025F03:P7. The tracer mass recovery for Yb-EDTA (KI0025F03:P6) is very high when calculated by integration but is much lower when calculated by weighing. Due to longer sampling time the mass recovery for Yb in test B-2a is higher (60 %) compared to He (48 %) injected at the same time. The mass recovery of Ho-DTPA from KA2563A:S1 only reaches about 35-45 %. Hence, a large portion of the tail of the breakthrough remains to be recovered and it is therefore likely that the mass recovery would have raised up to 50-65 % had the sampling been prolonged.

Table 3-8. Tracer mass recovery from pumping section KI0023B:P6 during test B-2.

Test #	Inj. Section	Structure #	Tracer	R_i (%)	R_w (%)	Sampling time (h)
B-2a	KI0025F03:P6	22, 20, 21	Helium	-	48	455
			Yb-EDTA	100	60	3073
B-2b	KI0025F02:P3	21	ReO_4	126	98	3235
B-2c	KA2563A:S1	19, 13, 21	Ho-DTPA	45	35	3234
B-2d	KI0025F03:P7	23, 20, 21	Gd-DTPA	114	88	3238
B-2e	KI0025F03:P3	21	In-EDTA	57	49	3239
B-2g	KI0025F03:P5	20, 21	Helium	-	97	184
			Naphtionate	121	100	252
B-2h	KI0025F02:P6	22, 20, 21	Rhodamine WT	42	49	548

R_i=recovery calculated by integration
R_w=recovery calculated by weighing

Helium test B-2a

The metal complex Yb-EDTA was used as reference tracer in Test B-2a. The observed breakthrough curves of the metal complex and He-3 show significant differences. The characteristics and a comparison of the two breakthrough curves are listed in Table 3-9. The He-peak concentration is lower and retarded compared to the reference tracer. The first arrival time of both tracers is approximately the same. Total mass recovery of both tracers is also about the same. The flow field KI0025F03:P6 –> KI0023B:P6 reveal an incomplete tracer breakthrough. About 50% recovery was calculated for both tracers. A projected 60% tracer recovery can be estimated by extrapolation in time of the measured breakthrough curves for both tracers.

Table 3-9. Results test B-2a.

	He-3	Reference tracer Yb-EDTA
First arrival [hrs]	50	51
Peak [hrs]	117	96
Peak C/Mo [1/ml]	$1.75\ 10^{-8}$	$2.44\ 10^{-8}$
Ratio $peak_{He}$ / $peak_{reftracer}$	0.72	0.72
Tracer recovery measured [%]	48.2	49.7
Tracer recovery extrapolated [%]	60%	60%
Duration of tracer input function [hrs]	48	48

The He-3 breakthrough peak signal was only about 27 % above the background signal. The relatively noisy raw data (at this very low concentration level) showed a correlation with temperature changes, which were indirectly observed by the photo multiplier background signal of the laser fluorometer. The He raw data were corrected for these temperature changes. In a second step, the He concentration data recorded every 5 minutes were reduced to an hourly average value (Figure 3-13).

No background drift of the He detector was observed during the entire test campaign. The presented He (hourly average) breakthrough and recovery curves (Figure 3-14 and 3-15) are based on the temperature corrections described above. The errors in the He measurements are most likely less than two times the fluctuation band of the data before averaging (about +/-10%).

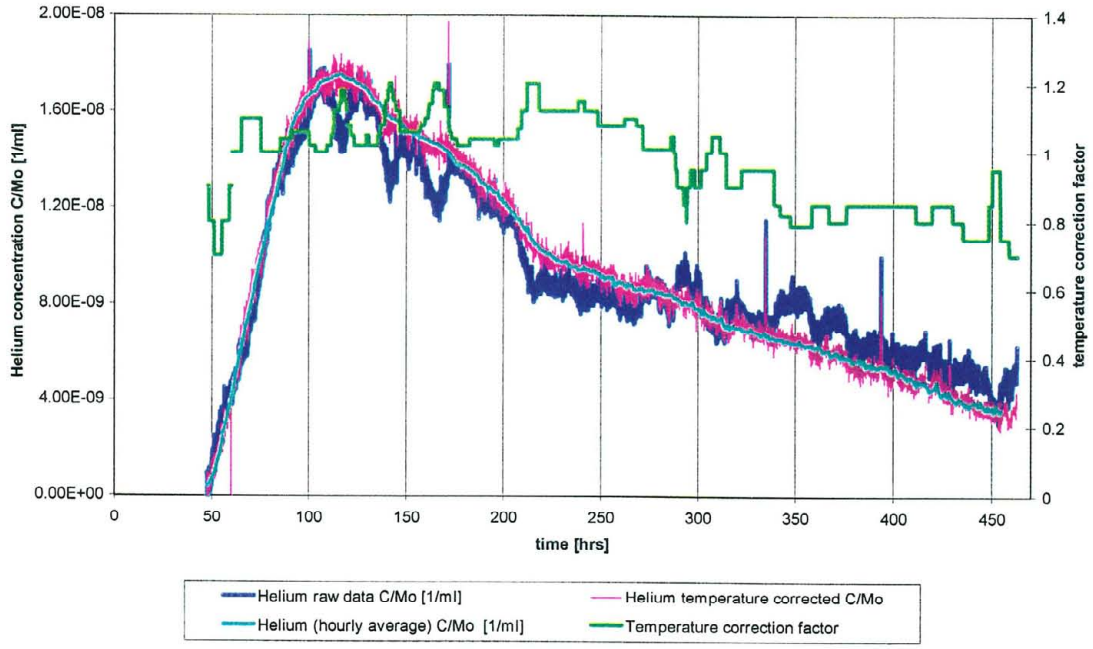

Figure 3-13. Temperature correction of raw data and hourly average of temperature corrected He-3 data.

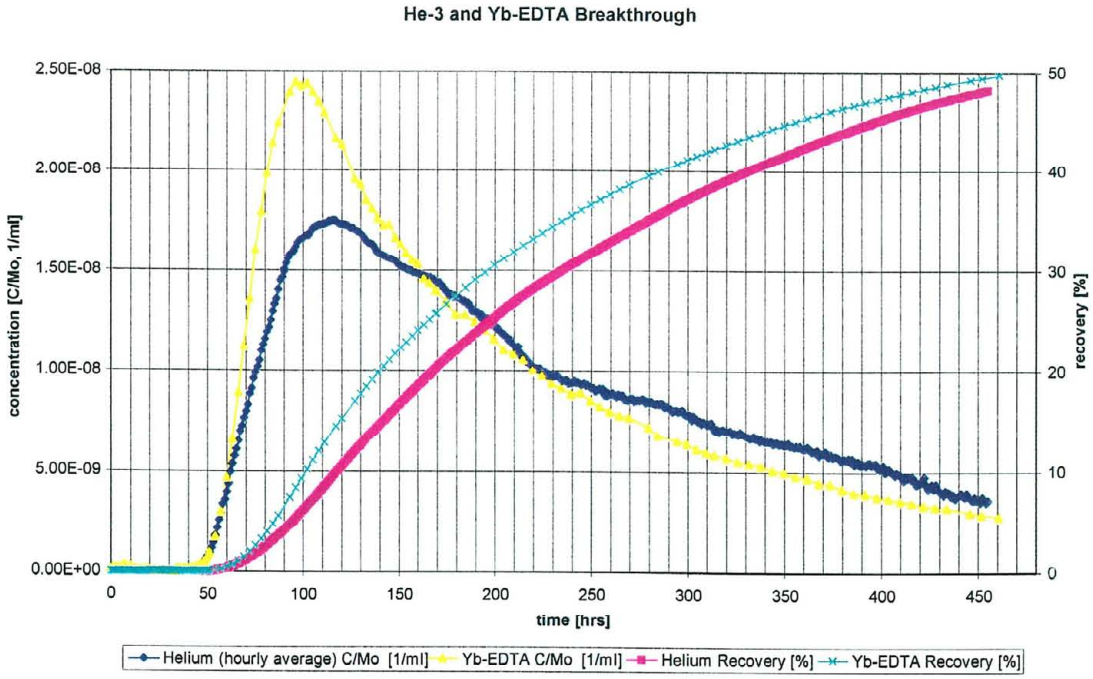

Figure 3-14. He-3 and Yb-EDTA breakthrough curves (linear scales), test B-2a.

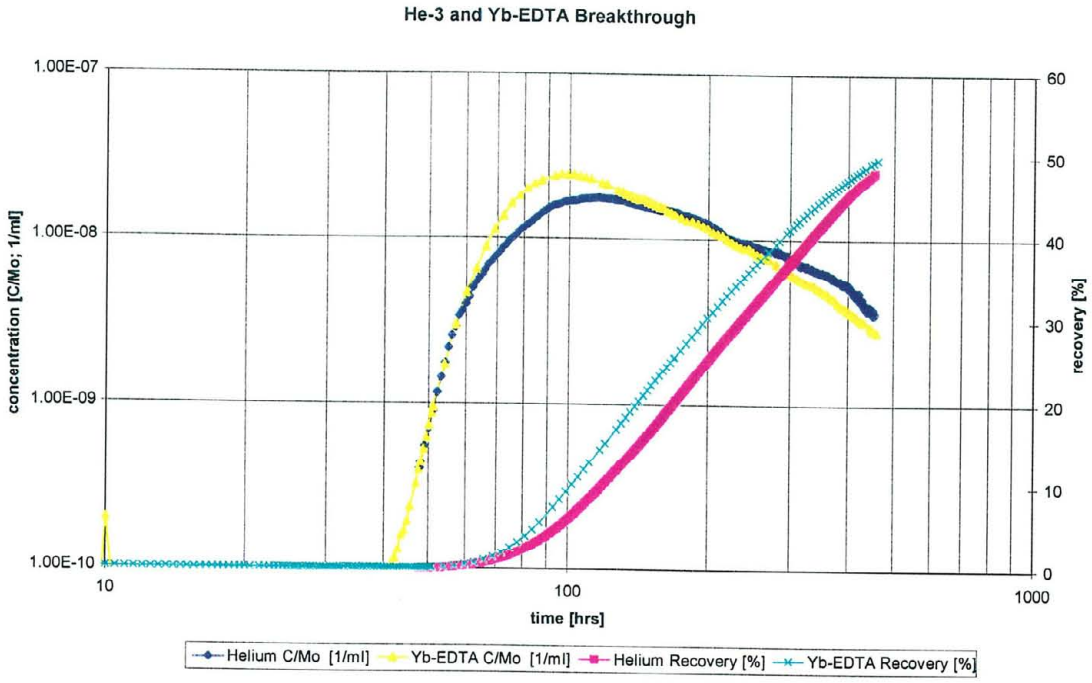

Figure 3-15. He-3 and Yb-EDTA breakthrough curves (logarithmic scales), test B-2a.

Helium test B-2g

The dye Naphtionate was used as reference tracer in test B-2g. The observed breakthrough curves of Naphtionate and He-3 showed significant differences. The characteristics and a comparison of the two breakthrough curves are listed in Table 3-10. The He-peak concentration is lower and retarded compared to the reference tracer. The first arrival time of both tracers is approximately the same. Total mass recovery of both tracers is also the same. The flow field KI0025F03:P5 –> KI0023B:P6 reveals a complete tracer breakthrough (as in Test B-1a performed in the same flow path).

Table 3-10. Results test B-2g.

	He-3	Reference tracer Naphtionate
First arrival [hrs]	4.8	4.5
Peak [hrs]	17.5	14.9
Peak C/Mo [1/ml]	$2.82\ 10^{-7}$	$3.81\ 10^{-7}$
Ratio $peak_{He}$ / $peak_{reftracer}$	0.74	0.74
Tracer recovery measured [%]	96	94
Tracer recovery extrapolated [%]	100%	100%
Duration of tracer input function [hrs]	13	13

The used Balzers He leak tester HLT 100 does not change the measurement range automatically. After first arrival, the He concentration increased rapidly and exceeded the lowest measurement range of the detector in the early morning (4:16) on the 23rd of May 2000 (10.6 hours after start of tracer dosage). During the morning of the 23rd, access to the test site was only possible by car through the access tunnel due to the weekly elevator check. Arriving on the test site was about 9:20. At 9:23 (elapsed time 15.7 hour) the measurement range was switched. As a consequence, the He breakthrough was not monitored during 5 hours. Figure 3-16 illustrates the interpolation of the missing data of the He breakthrough curve. The breakthrough curves are presented in Figure 3-17 and 3-18.

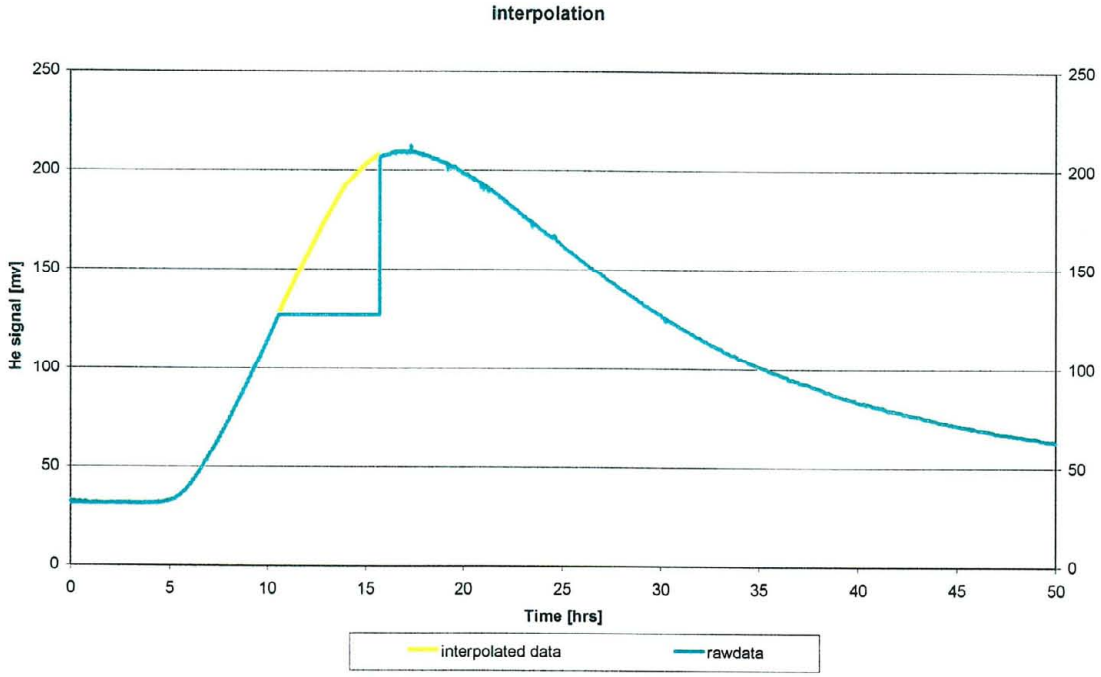

Figure 3-16. Interpolation of missing He-3 data.

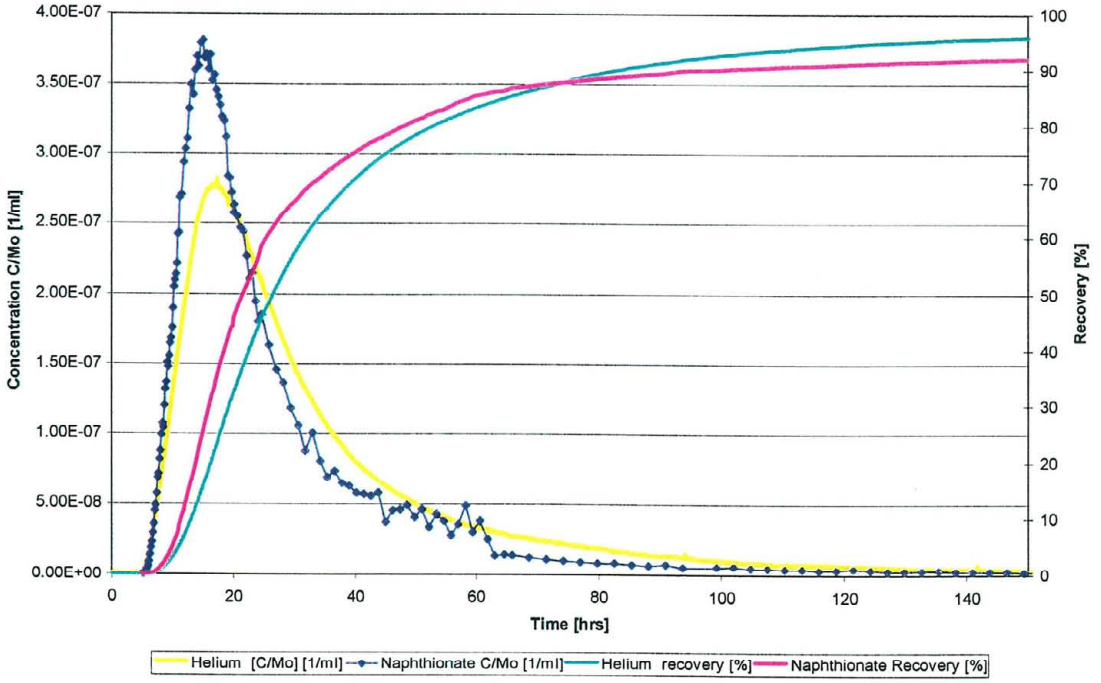

Figure 3-17. He-3 and Naphtionate breakthrough curves (linear scales).

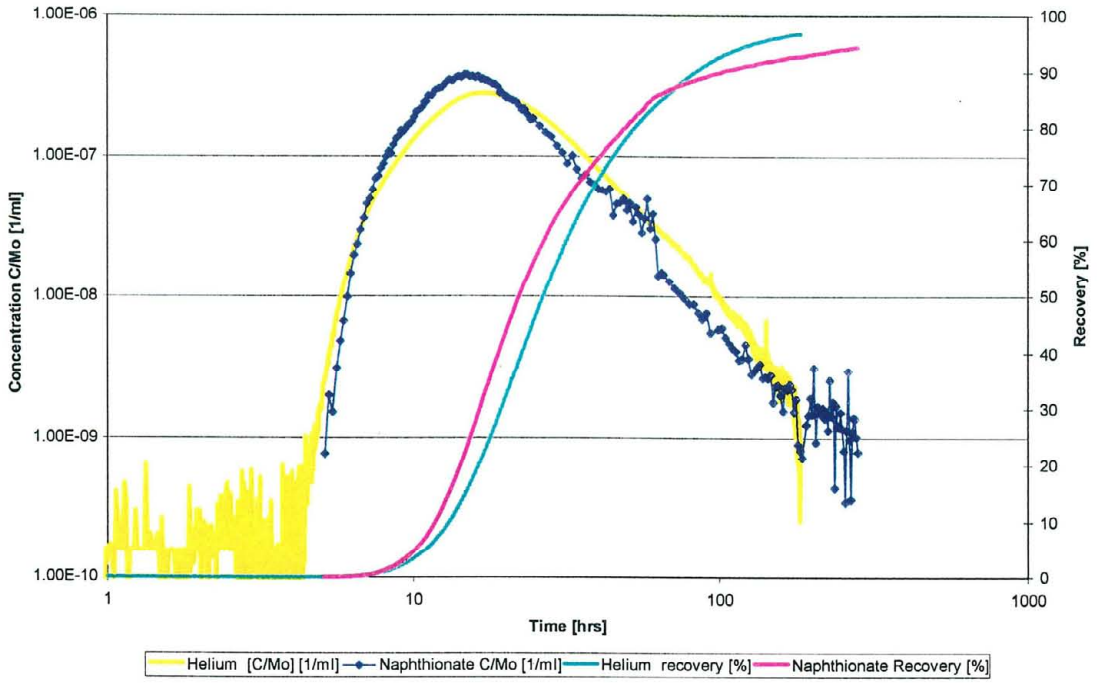

Figure 3-18. He-3 and Naphtionate breakthrough curves (logarithmic scales)

3.4.3 Numerical modelling and analytical interpretation

The breakthrough curves from B-2 were evaluated using the one-dimensional advection-dispersion model described in Section 2.5.2.The transport parameters derived from the numerical modelling and the analytical expressions described in Section 2.5.2 are presented in Table 3-11.

The best-fit runs for each tracer/flow path are presented in Figure 3-19. The modelling resulted in fits with quite low standard errors, 1-5 %. In general the peak of the breakthrough curves is quite well fitted while the fit of the tail part is not as good. The modelling could most likely be improved either by including transport though one or more additional flow path(s) or by including other processes like diffusion into stagnant areas or diffusion into the rock matrix. However, this was beyond the scope of this initial modelling effort.

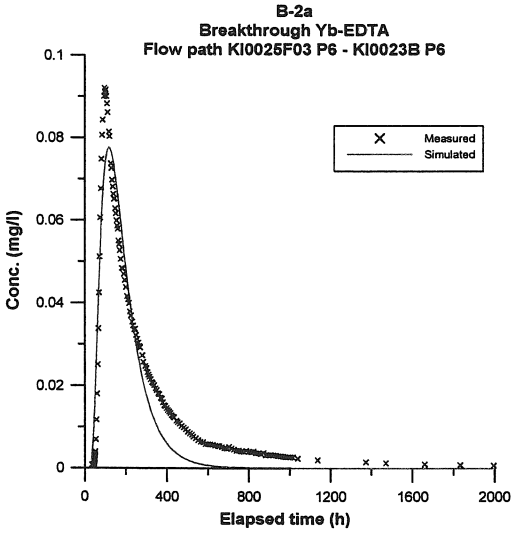
B-2a
Breakthrough Yb-EDTA
Flow path KI0025F03 P6 - KI0023B P6
Measured
Simulated
Conc. (mg/l)
Elapsed time (h)

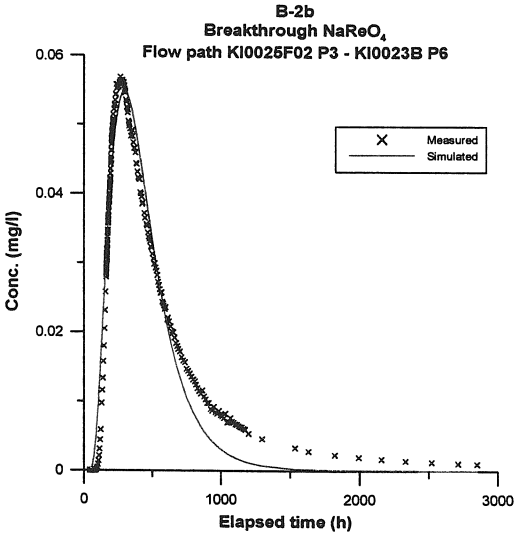
B-2b
Breakthrough NaReO4
Flow path KI0025F02 P3 - KI0023B P6
Measured
Simulated
Conc. (mg/l)
Elapsed time (h)

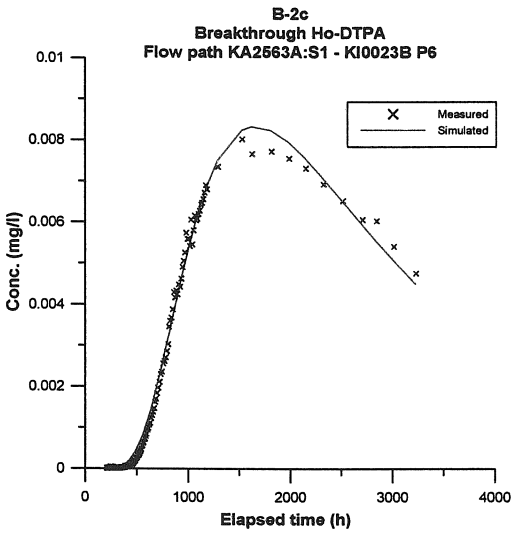
B-2c
Breakthrough Ho-DTPA
Flow path KA2563A:S1 - KI0023B P6
Measured
Simulated
Conc. (mg/l)
Elapsed time (h)

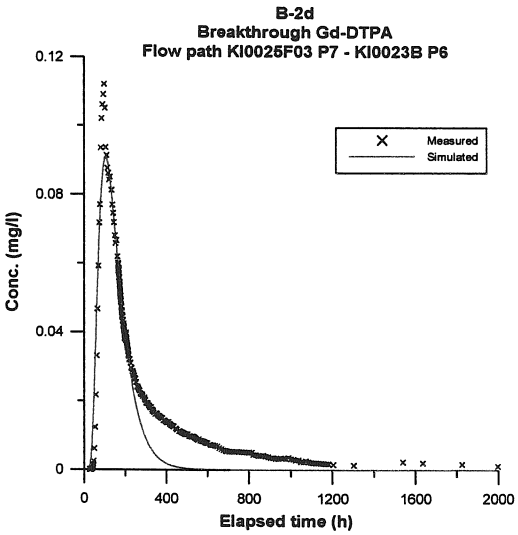
B-2d
Breakthrough Gd-DTPA
Flow path KI0025F03 P7 - KI0023B P6
Measured
Simulated
Conc. (mg/l)
Elapsed time (h)

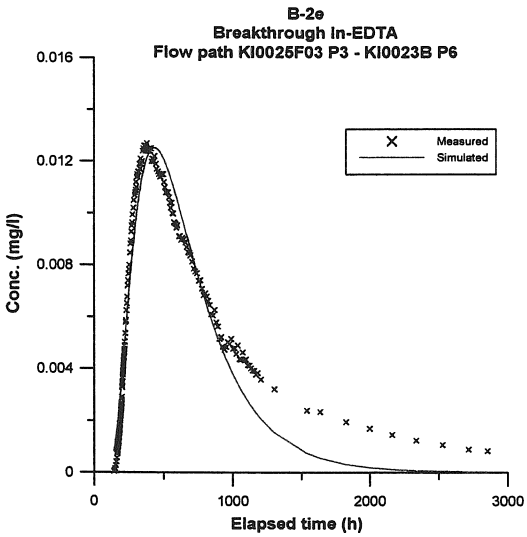
B-2e
Breakthrough In-EDTA
Flow path KI0025F03 P3 - KI0023B P6
Measured
Simulated
Conc. (mg/l)
Elapsed time (h)

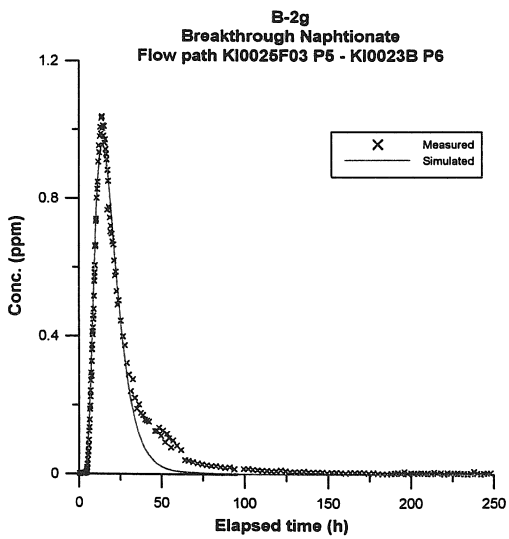
B-2g
Breakthrough Naphtionate
Flow path KI0025F03 P5 - KI0023B P6
Measured
Simulated
Conc. (ppm)
Elapsed time (h)

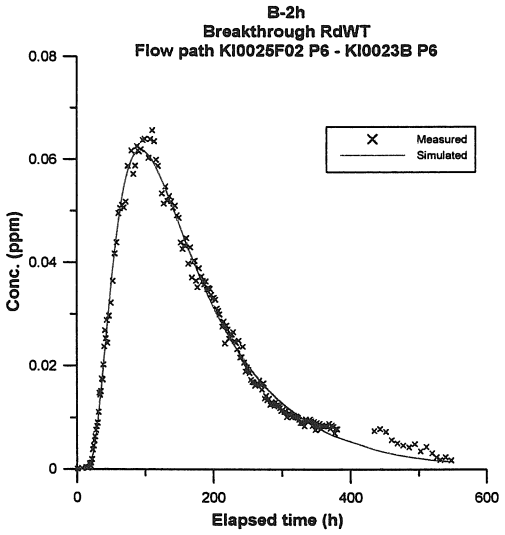

Figure 3-19. Comparison between measured and simulated tracer breakthrough in KI0023B:P6 during test B-2, cf. Table 3-11 for evaluated parameters. Note that the axis scales differ between the plots.

Table 3-11. Summary of hydraulic and transport parameters for the flow paths tested in B-2 using KI0023B:P6 as sink. Values within brackets are standard errors in percent.

Parameter/ Injection section	B-2a KI0025 F03:P6	B-2b KI0025 F02:P3	B-2c KA2563 A:S1	B-2d KI0025 F03:P7	B-2e KI0025 F03:P3	B-2g KI0025 F03:P5	B-2h KI0025 F02:P6	Source
Distance along fractures (m)	73	33	>55	97	27	16	65	Geometry
Euclidean distance, L (m)	15	33	55	17	27	14	18	Geometry
Mean head difference, Δh (m)	182.3	185.7	186.6	178.3	187.1	164.4	177.9	HMS
Inj. flow rate (ml/h)	714	95	30	502	575	2039	761	Injection curve
Mean velocity, v (m/s)	$2.83 \cdot 10^{-5}$ (2)	$3.20 \cdot 10^{-5}$ (1)	$7.0 \cdot 10^{-6}$ (1)	$3.97 \cdot 10^{-5}$ (1)	$1.34 \cdot 10^{-5}$ (1)	$2.87 \cdot 10^{-4}$ (1)	$4.07 \cdot 10^{-5}$ (1)	PAREST
Mean travel time, t_m (h)	147.2 (2)	286.4 (1)	2182 (1)	118.9 (1)	561.0 (1)	13.5 (1)	122.7 (1)	PAREST
First arrival, t_a (h)	44	83	450	43	150	4.5	21	Break-through curve
Dispersivity, D/v (m)	2.7 (5)	7.0 (3)	12.8 (1)	2.4 (4)	4.5 (2)	1.9 (3)	5.4 (2)	PAREST
Peclet number, Pe	5.6	4.7	4.3	7.1	6.1	7.3	3.3	PAREST
Fracture conductivity, K_{fr} (m/s)	$7.0 \cdot 10^{-6}$	$1.9 \cdot 10^{-5}$	$7.8 \cdot 10^{-6}$	$1.2 \cdot 10^{-5}$	$6.3 \cdot 10^{-6}$	$7.2 \cdot 10^{-5}$	$1.3 \cdot 10^{-5}$	Eq. 2-4
Equivalent fracture aperture, b (m)	$2.6 \cdot 10^{-2}$	$1.0 \cdot 10^{-2}$	$2.8 \cdot 10^{-2}$	$1.6 \cdot 10^{-2}$	$3.0 \cdot 10^{-2}$	$2.7 \cdot 10^{-3}$	$1.5 \cdot 10^{-2}$	Eq. 2-5
Flow porosity (1 m thickness)	$1.5 \cdot 10^{-2}$	$5.5 \cdot 10^{-3}$	$1.5 \cdot 10^{-2}$	$9.1 \cdot 10^{-3}$	$1.7 \cdot 10^{-2}$	$1.5 \cdot 10^{-3}$	$8.2 \cdot 10^{-3}$	Eq. 2-6
Mass recovery, R (%)	100 60*	126 98*	45 35*	114 88*	57 49*	121 100*	42 49*	Break-through curve

*=recovery calculated by weighing

4 Discussion and conclusions

4.1 Performance of tests

4.1.1 Experimental techniques

The Phase B tracer tests have involved ten tracer injections using ten different tracers in eight different flow paths. The main difference with these tests compared to earlier tracer tests in the TRUE Block Scale Project is that most of the tracer injections have been performed with a forced gradient (unequal dipole). The main reason for using this technique has been to increase the mass flux at the injection points and thereby also increase the possibility of detecting the tracer at the sink. Earlier tracer injections have preferably been performed in sections having high induced groundwater flow (measured by tracer dilution tests), while in Phase B most injection sections had low induced flow. This strategy turned out quite well as tracer breakthrough was observed from all ten injections.

The main drawback of the forced injection is that an injection pump is needed at each injection point. This pump should be designed to maintain a relatively low and stable injection flow rate over periods of months in a rough environment (corrosive chemistry, particles, etc.). The pumps used in Phase B, plunger pumps designed for laboratory use, did not withstand the difficult conditions in the tunnel. Not only the environment but also the high pressure and the water chemistry made it difficult to maintain constant injection over longer periods than two-three weeks at the most. For future tests this problem needs to be resolved either by using pumps of industrial type, or by creating the forced gradient with nitrogen gas and a flow regulator similar to the one used for maintaining the constant flow at the sink.

The Phase B tracer tests also included Helium (He-3) injections using equipment and techniques developed by SOLEXPERTS AG for the Grimsel tracer experiments (Frick et al, 1991). This equipment included in-line detection of Uranine in the injection and pumping sections as well as in-line detection of Helium in the pumping section. Also for this equipment similar problems with the injection pump occurred as a result of the difficult conditions at the site. The in-line detection of Uranine worked well but could not measure higher injection concentrations than 10 ppm, which was too low to get breakthrough concentrations above the background level at the site. It should also be noted that the background level was about 10-100 times higher than normal due to contamination from previously performed tracer tests with Uranine at the site.

The Helium detection equipment worked well although it is rather sensitive to the temperature at the site. This, in combination with breakthrough concentrations close to the background level, made it necessary to correct for temperature effects.

The borehole instrumentation worked well with one exception. During tracer injection in KI0025F02:P6 the circulation flow rate decreased and the pressure in the flow line increased. Since no pressure build-up was monitored in the section this could only be caused by an equipment defect in the flow line between the circulation pump and the outlet into the borehole section. The most probable explanation is that the sintered filter at the outlet was clogged. The reason for this is currently not known but will be examined when the borehole equipment is removed.

All other components of the injection and sampling system worked well throughout the tests.

4.1.2 Tracer behaviour

Already early in the project a need for conservative tracers was identified. This resulted in a relatively elaborate literature search and field test campaign of a number of candidate tracers (Holmqvist et al., 2000). The study, also including a feasibility test of Helium, selected about 20 different conservative tracers, of which about ten were stable rare-earth metal complexes, to be used in tracer tests at Äspö HRL. The Phase B tests shows that the selected tracers (four different metal complexes, perrhenate, and four fluorescent dyes, cf. Tables 3-3 and 3-7) seem to be stable and conservative. The latter was checked by adding Amino G Acid to the injection solutions as a reference tracer in all injection sections. However, no signs of reactive behaviour could be seen. The behaviour of Helium is discussed below.

4.2 Transport in block scale

In total eight different flow paths using the same sink, KI0023B:P6, were tested. Therefore, only the label of the injection section will denote the flow paths in the following text. Two of the flow paths (KI0025F03:P5 and P6) were also tested at two different pumping rates (1.2 and 2.1 l/min, respectively). The basic idea using a lower pumping rate was to increase the possibility of observing diffusion effects.

The results of the tracer tests are discussed below in relation to their objectives and the hypotheses tested. Note that the analysis is based only on the basic interpretation described in this report. Further analysis of the data is beyond the scope of this report but will be made later as a part of the final evaluation of the TRUE Block Scale Tracer Test Stage.

4.2.1 Diffusion effects

Four of the Phase B tests were performed with the objective to study diffusion effects (B-1a, B-1b, B-2a, and B-2g). The tests were performed in two different pathways, one "single" fracture path (KI0025F03:P5) and one "network" path (KI0025F03:P6). Three of the injections also included Helium (He-3) having a significantly higher diffusivity than the reference tracers (dyes or metal complexes).

In test B-1a (KI0025F03:P5) the Helium breakthrough could unfortunately not be compared to the reference tracer (Uranine) due to the low input concentration in combination with high background. However, according to Hadermann & Heer (1996) matrix diffusion may be identified by the slope of the late-time part of the breakthrough curve. A slope of $t^{-3/2}$ indicates diffusion in a double-porosity medium. In test B-1a the slope is steeper, about $t^{-5/2}$ (cf. Figure 3-6), but still not as steep as would have been the case if only advection and dispersion were considered. Test B-1b (KI0025F03:P6) shows a slope of $t^{-3/2}$ thus indicating diffusion effects.

In both runs, B-2a (KI0025F03:P6) and B-2g (KI0025F03:P5), He and the reference tracer breakthrough curves show the following characteristics (cf. Figures 3-15 and 3-18):

- lower He peak concentration
- retarded He peak
- more marked tailing
- similar tracer recovery

The first part of the tracer breakthrough curves (simultaneous first arrival of Helium and the reference tracer and the steep rising part of the breakthrough curves) is probably governed by rapid advective transport in highly transmissive flow channels.

The lower and retarded He peak indicates that diffusion as a transport process is accentuated by the more diffusive He. The longer tailing of the He breakthrough curve can also be explained by the more diffusive He. The similar tracer recovery measured for He and the reference tracers indicate that no sorption processes biased the experiments.

A comparison of the two flow paths investigated for diffusion effects, the "single fracture path" KI0025F03:P5 (tests B-1a and B-2g), and the "network path" KI0025F03:P6 (tests B-1b and B-2a) is shown in Figure 4-1. The figure reveals some interesting differences and similarities between the two paths. Firstly, the mean travel time is about 10 times longer for the "network" flow path although the closest (Euclidean) distance is almost the same. This indicates that the flow path KI0025F03:P6 indeed represents a "network path". Secondly, the difference in first arrival and peak travel time caused by the changed pumping rate is similar for both flow paths. The travel time in a radial flow system is governed by the hydraulic gradient and in this case the change in gradient due to the changed pumping rate is similar for both flow paths and thus consistent with the breakthrough curves.

The third interesting difference between the curves is the slope of the tail which is already discussed above. The "single fracture path" has a slope of $t^{-5/2}$ while the "network path" has a slope of $t^{-3/2}$ and the slope is the same for both pumping rates. Thus, the lower pumping rate did not increase the possibility to detect diffusion effects in this case.

Finally, it should be noted that the simple analysis made in this report can not be used as an evidence that we really see diffusion effects. Not even the bad model fits obtained with the simple advection-dispersion model used in this report is an evidence for such effects. A more thorough analysis, beyond the scope of this report is needed, where effects that may give similar results (e.g. heterogeneity, multiple flow paths) are considered. Another explanation for the difference may be effects of fracture intersection zones (FIZ) and this will be further analysed as a part of the TRUE Block Scale Evaluation and Reporting Stage (ERS).

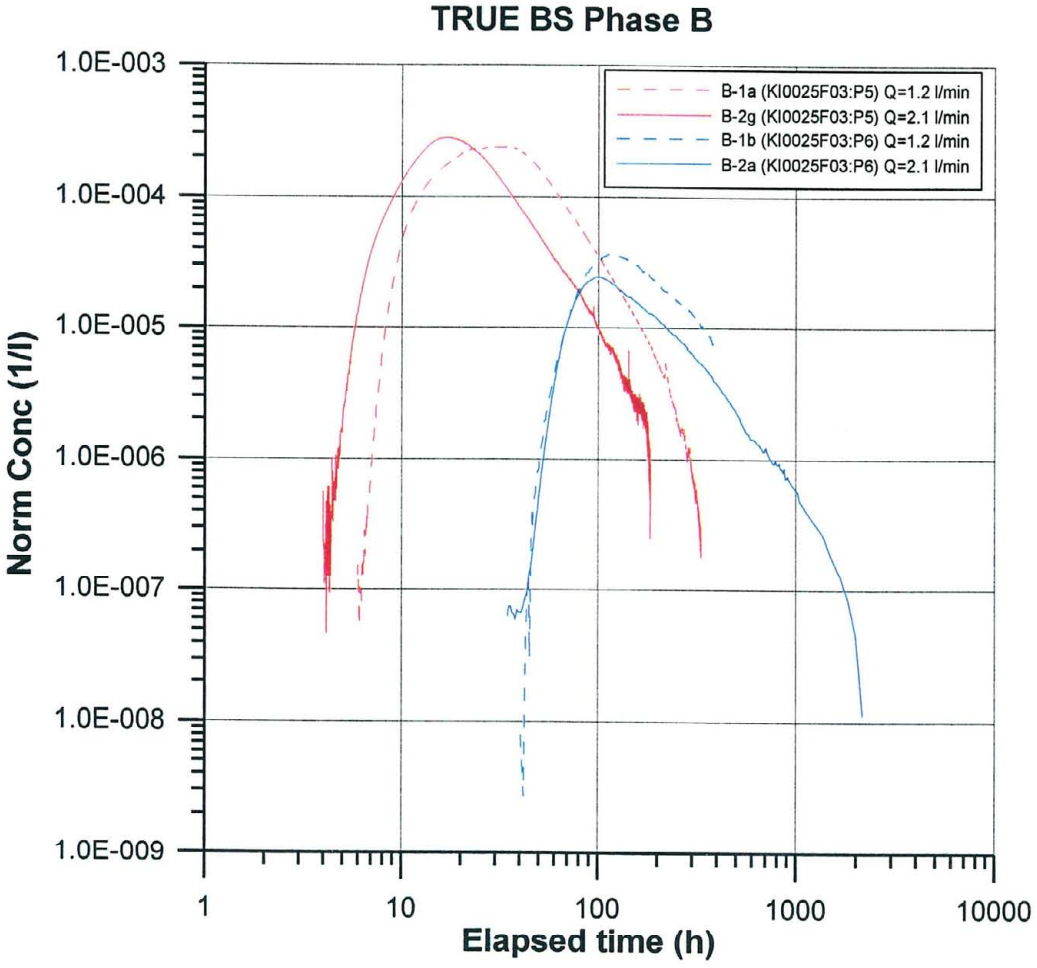

Figure 4-1. Comparison between tracer breakthrough from injection in KI0025F03:P5 and KI0025F03:P6 at two different pumping rates (Q=1.2 and 2.1 l/min, respectively).

4.2.2 Transport in network vs. single fractures

Figure 4-2 shows a plot of all seven breakthrough curves from runs B-2a though B-2g. Four of the seven flow paths tested represent "network paths" (B-2a, c, d and h) whereas the three remaining represent "single fracture paths" (B-2b, e and g). By studying the breakthrough curves in combination with the parameters derived from the interpretation (Table 3-11) some observations can be made:

- Flow path KI0025F03:P5 is fast and has a low dispersivity (1.9 m) indicating mostly advective transport (also indicated by a steep tailing, $t^{-5/2}$) and that the "true" travel distance is close to the geometrical one, i.e. a "single fracture path".

- The three "network flow paths" KI0025F03:P6, KI0025F03:P7 and KI0025F02:P6 have similar geometric path lengths (15-18 m) as the "single fracture path" (KI0025F03:P5) but path lengths according to the structural model between 65-97 m. All three breakthrough curves are significantly delayed and have higher dispersivity than the "single fracture path" indicating transport through a network. The slopes of the tails are less steep ($t^{-3/2}$-$t^{-4/2}$) which may indicate that transport is more affected by diffusion than in the "single fracture path".

- Flow path KA2563A:S1 has an even longer travel time, a very high dispersivity (12.8 m) and is undoubtedly a "network path" involving at least three structures. It is likely that the true travel distance is well beyond 100 meters. The slope of the tail can not be evaluated as only a very short part of the tail had been recovered at end of the sampling period (3000 hours).

- The two remaining flow paths, KI0025F02:P3 and KI0025F03:P3, are both "single fracture paths" having path lengths of 33 and 27 m, respectively, according to the structural model. However, both paths are slow, have high dispersivity (4.5-7.0 m) and less steep tails ($t^{-3/2}$) i.e. similar to the "network paths". Path KI0025F03:P3 is particularly slow although the travel distance is much shorter than the "network paths". This path is also interpreted to be close to a fracture intersection and one explanation could be that transport occurs along this intersection having an enhanced pore volume and thus, decreasing the transport velocity. Another explanation may be that the structure (#21) is discontinuous or consists of several sub-parallel structures making up a much longer travel distance than the geometrical one.

In summary, the interpretation of the flow paths is generally consistent with the present structural model (Hermanson & Doe, 2000). However, the longer (25-35 m) "single fracture paths" are most probably made up of more than one single fracture.

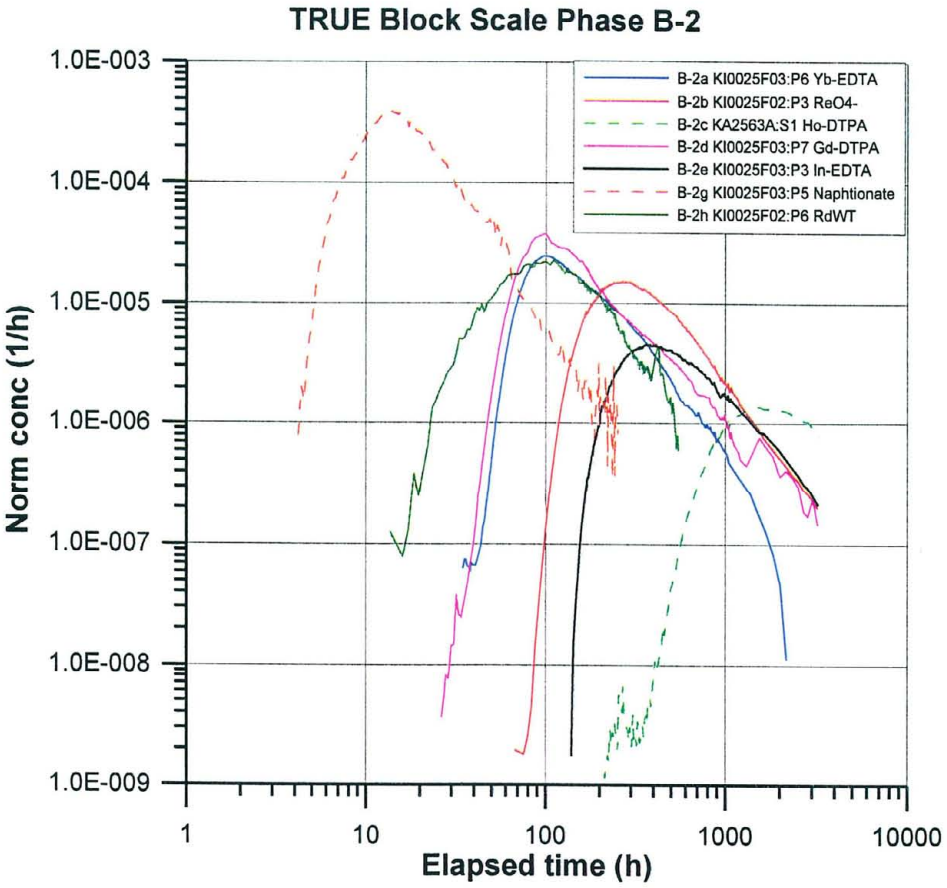

Figure 4-2. Comparison of tracer breakthrough from all seven tracer injections during Phase B-2 (logarithm of normalised concentration versus logarithm of elapsed time).

4.3 General conclusions

The TRUE Block Scale Phase B tracer tests have involved a multitude of tracers in a multitude of different injection schemes within a relatively short time. The results of the tests were generally good, meaning that data of high quality could be produced for a number of different flow paths over distances between 15 to at least 100 meters. Given the results and conclusions presented above the general objective to "increase the understanding of transport in block scale" has been met although a complete understanding still is far away. The tracer retention aspect (through diffusion) has been enlightened by the use of Helium.

The tests have also provided an input for selection of flow paths suitable for further studies with sorbing tracers (Phase C). A recommendation (and possibly also a requirement) is to use flow paths with high tracer mass recovery. Based on the results presented in this report such flow paths are KI0025F03:P5, KI0025F03:P7 and KI0025F02:P3 (sink in KI0023B:P6).

5 References

Andersson, P., 1996: TRUE 1st stage tracer test programme. Experimental data and preliminary evaluation of the TRUE-1 radially converging tracer test (RC-1). Äspö Hard Rock Laboratory Progress Report HRL-96-24.

Andersson, P., Ludvigson, J-E., Wass, E., Holmqvist, M., 1999: TRUE Block Scale Project, Detailed Characterisation Stage. Interference tests and tracer tests, PT-1 - PT-4. Äspö Hard Rock Laboratory International Technical Document ITD-99-19.

Andersson, P., Ludvigson, J-E., Wass, E., Holmqvist, M., 2000: TRUE Block Scale Project Tracer Test Stage. Interference tests, dilution tests and tracer tests, Phase A. Äspö Hard Rock Laboratory International Progress Report IPR-00-28.

Frick, U., Alexander, W.R., Bayens, B., Bossart, O., Bradbury, M.H., Bühler, C., Eikenberg, J., Fierz, T., Heer, W., McKinley, I. and Smith, P., 1992: Grimsel Test Site: The radionuclide migration experiment, overview of investigations 1985 – 1990. Nagra Technical Report 91-04, Wettingen Switzerland.

Gustafsson, E., Klockars, C-E., 1981: Studies of groundwater transport in fractured crystalline rock under controlled conditions using non-radioactive tracers. Swedish Nuclear Fuel and Waste Management Company. SKBF/KBS Technical Report TR 81-07.

Hadermann, J., Heer, W., 1996: The Grimsel (Switzerland) migration experiment: integrating field experiments, laboratory investigations and modelling. Journal of Contaminant Hydrology 21 (1996), 87-100.

Hermanson, J., Doe, T., 2000: TRUE Block Scale Project. March´00 Structural and Hydraulic Model Based on Borehole Data from KI0025F03. SKB International Progress Report IPR-00-34.

Holmqvist, M., Andersson, O., Trick, T., Fierz, T., Eichinger, L., Scholtis, A., 2000: TRUE Block Scale Project. Test of new possible non-reactive tracers – experimental description and evaluation. Äspö Hard Rock laboratory International Technical Document ITD-00-07.

Moye, D.G., 1967: Diamond drilling for foundation exploration. Civil Eng. Trans., Inst. Eng. Australia (Apr. 1967), 95-100.

Nordqvist, R., 1994: Documentation of some analytical flow and transport models implemented for use with PAREST - Users manual. GEOSIGMA GRAP 94 006, Uppsala.

Ogata, A., Banks, R., 1961: A solution to the differential equation of longitudinal dispersion in porous media. U.S. Geol. Surv. Prof. Paper 411-A, Washington.

Van Genuchten, M.Th., 1982: One-dimensional analytical transport modeling, in Proceedings: Symposium on unsaturated flow and transport modeling. Rep. PNL-SA-10325, Pacific Northwest Lab., Richland, Washington

Van Genuchten M.Th., and Alves, W.J., 1982: Analytical solutions of the one-dimensional convective-dispersive solute transport equation. U.S. Dep. Agric. Tech. Bull. 1661.

Winberg A. (ed), 1996: First TRUE Stage - Tracer Retention Understanding Experiments. Descriptive structural-hydraulic models on block and detailed scales of the TRUE-1 site. Swedish Nuclear Fuel and Waste Management Company. Äspö Hard Rock Laboratory International Cooperation Report ICR 96-04.

Winberg, A., 1997: Test plan for the TRUE Block Scale Experiment. Äspö HRL International Cooperation Report ICR 97-02.

Winberg, A. (ed), 2000: TRUE Block Scale Project. Tracer Test Stage. Compilation of premises and outline of programme for tracer tests in the Block Scale. Äspö Hard Rock Laboratory International Cooperation Report ICR-00-02.

Zuber, A., 1974: Theoretical possibilities of the two-well pulse method. Isotope Techniques in Groundwater Hydrology 1974, Proc. Symp., Vienna 1974, IAEA, Vienna

APPENDIX 1: Breakthrough and injection curves as mass flux versus time for B-1 and B-2

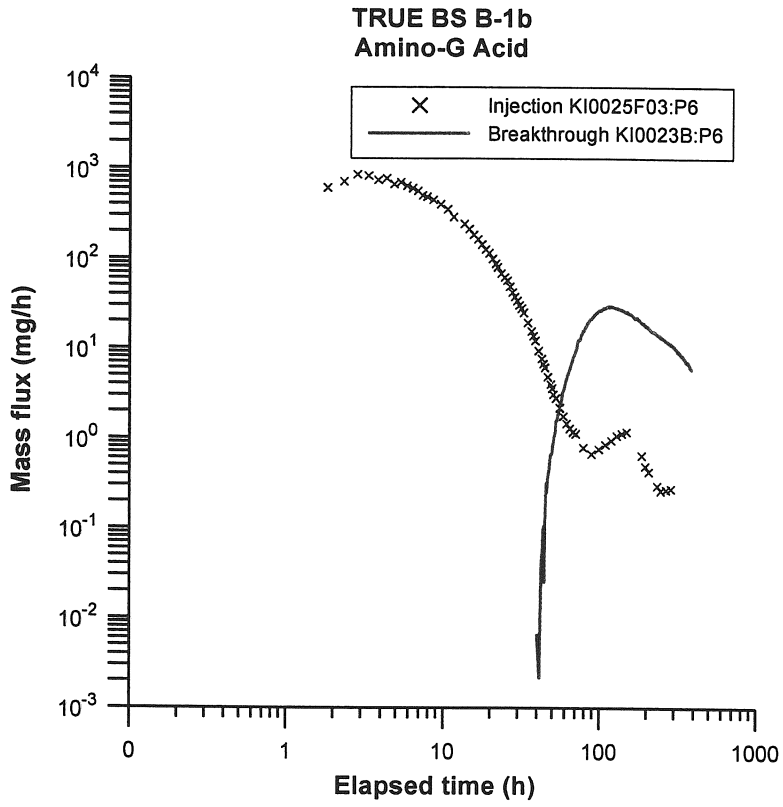
TRUE BS B-1b
Amino-G Acid
Injection KI0025F03:P6
Breakthrough KI0023B:P6
Mass flux (mg/h)
Elapsed time (h)
10^4
10^3
10^2
10^1
10^0
10^-1
10^-2
10^-3
0
1
10
100
1000

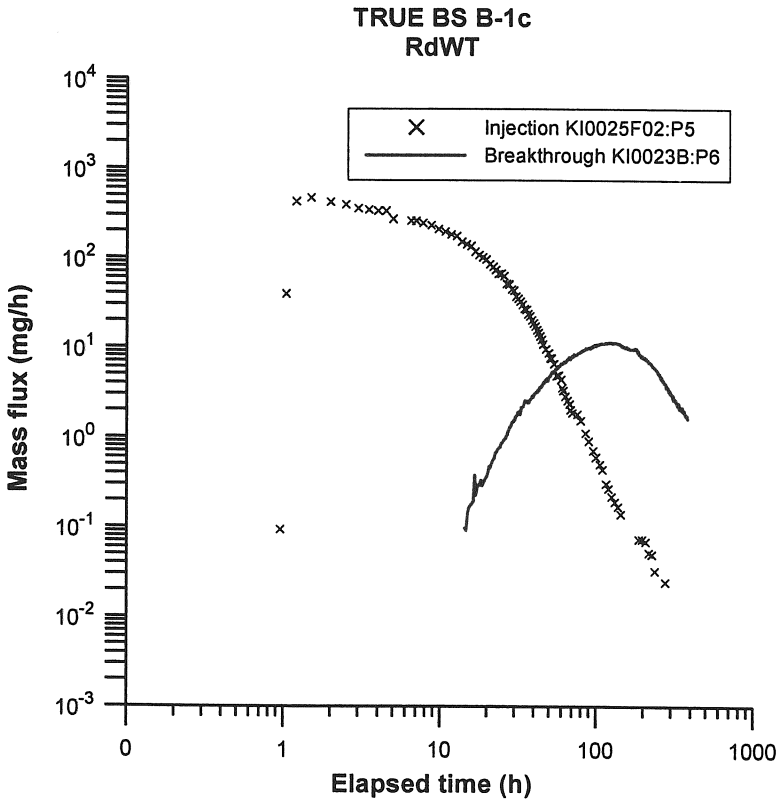
TRUE BS B-1c
RdWT
Injection KI0025F02:P5
Breakthrough KI0023B:P6
Mass flux (mg/h)
Elapsed time (h)
10^4
10^3
10^2
10^1
10^0
10^-1
10^-2
10^-3
0
1
10
100
1000

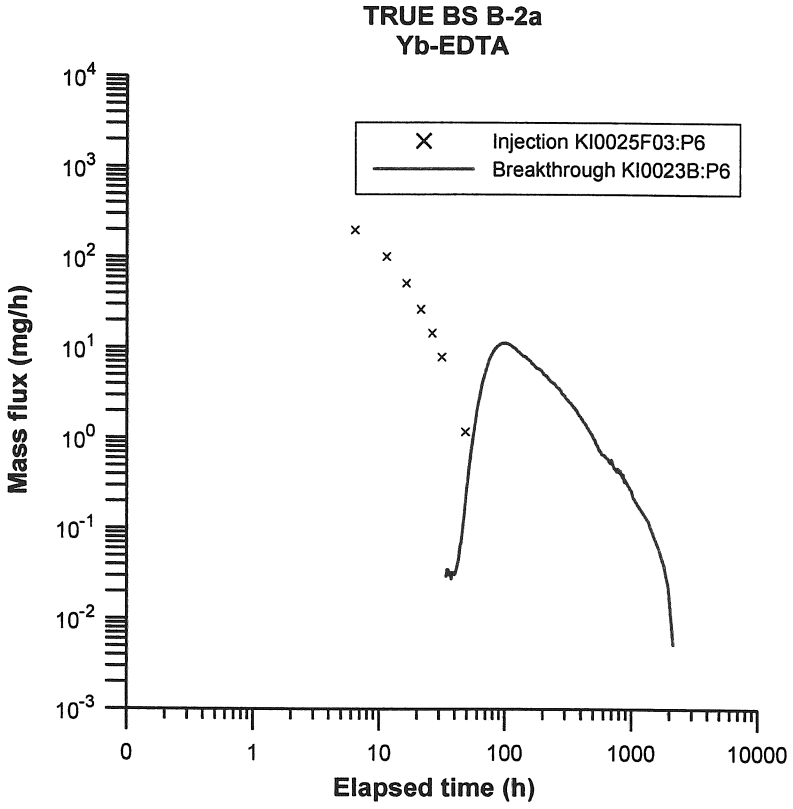
TRUE BS B-2a
Yb-EDTA
Injection KI0025F03:P6
Breakthrough KI0023B:P6
Mass flux (mg/h)
Elapsed time (h)

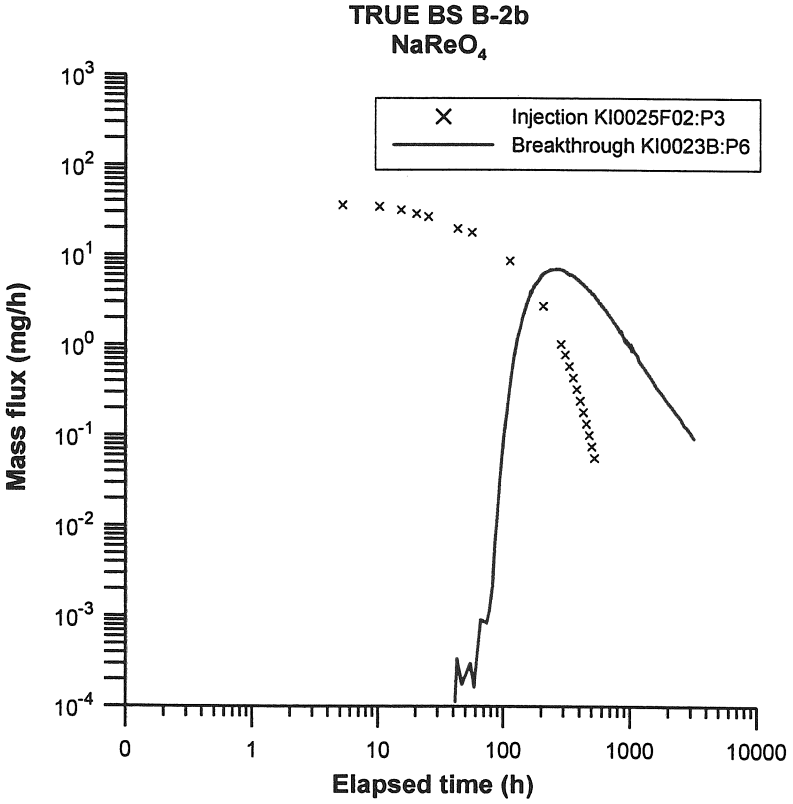
TRUE BS B-2b
NaReO4
Injection KI0025F02:P3
Breakthrough KI0023B:P6
Mass flux (mg/h)
Elapsed time (h)

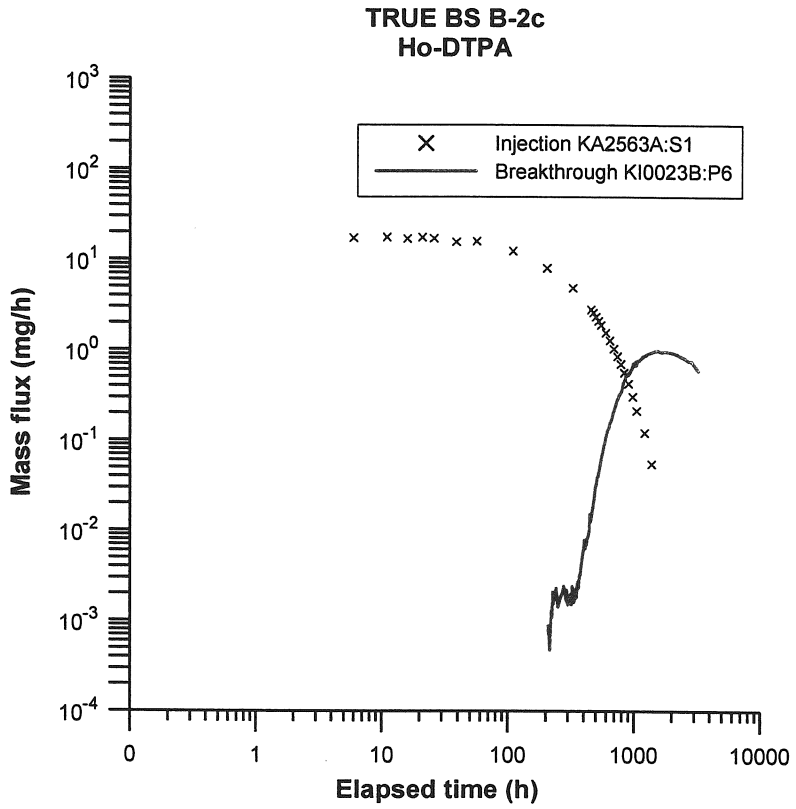
TRUE BS B-2c
Ho-DTPA
Injection KA2563A:S1
Breakthrough KI0023B:P6
Mass flux (mg/h)
Elapsed time (h)
10^3
10^2
10^1
10^0
10^-1
10^-2
10^-3
10^-4
0
1
10
100
1000
10000

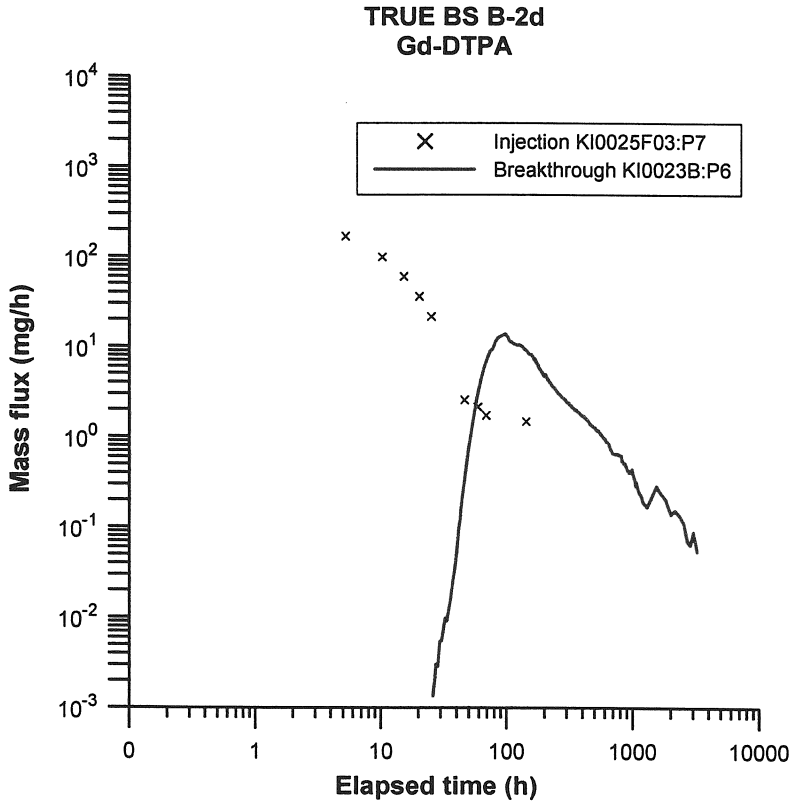
TRUE BS B-2d
Gd-DTPA
Injection KI0025F03:P7
Breakthrough KI0023B:P6
Mass flux (mg/h)
Elapsed time (h)
10^4
10^3
10^2
10^1
10^0
10^-1
10^-2
10^-3
0
1
10
100
1000
10000

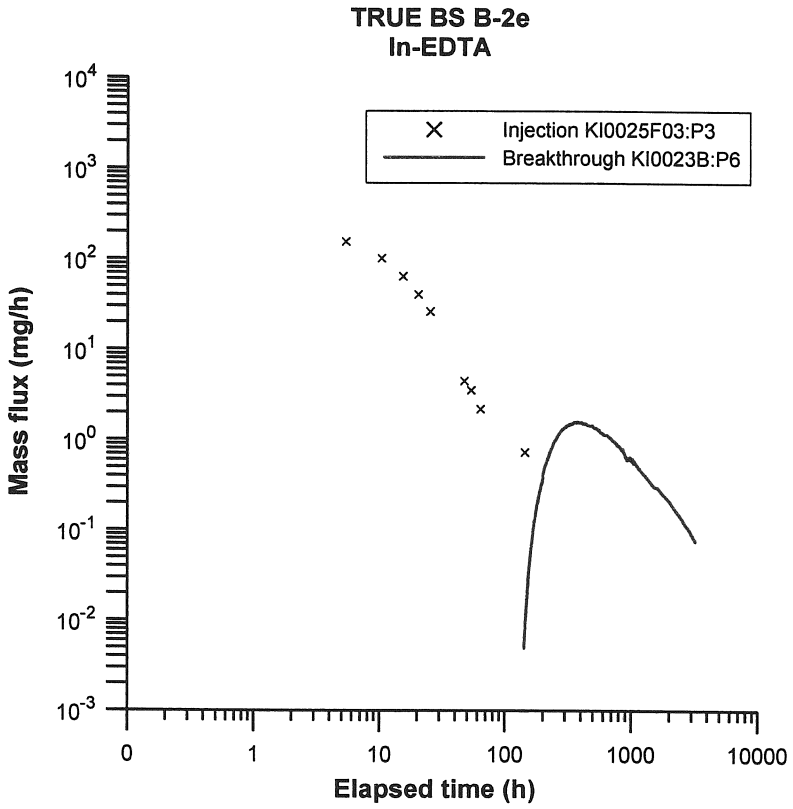
TRUE BS B-2e
In-EDTA
Injection KI0025F03:P3
Breakthrough KI0023B:P6
Mass flux (mg/h)
Elapsed time (h)
10^4
10^3
10^2
10^1
10^0
10^-1
10^-2
10^-3
0
1
10
100
1000
10000

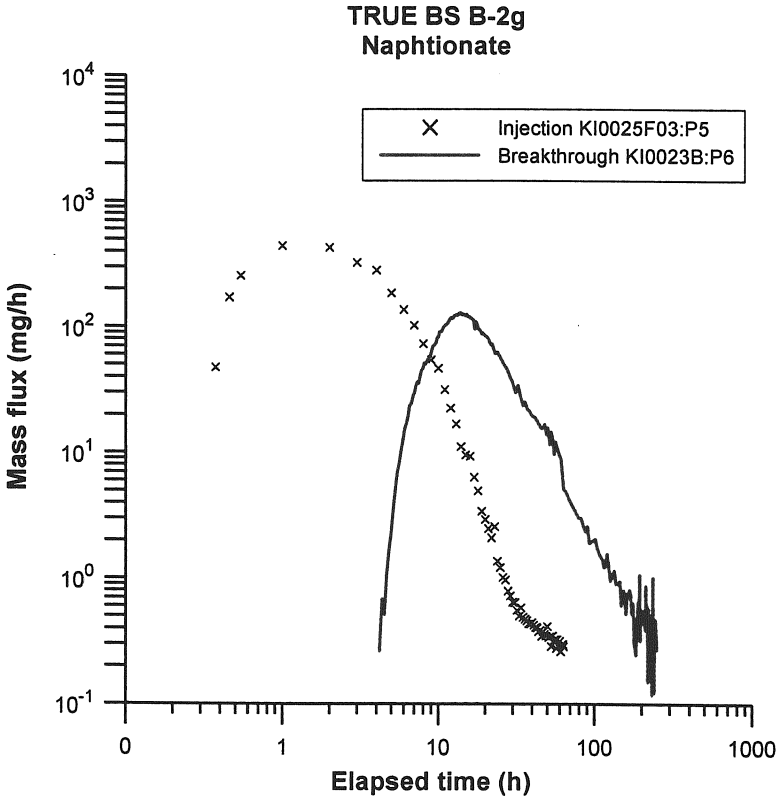
TRUE BS B-2g
Naphtionate
Injection KI0025F03:P5
Breakthrough KI0023B:P6
Mass flux (mg/h)
Elapsed time (h)
10^4
10^3
10^2
10^1
10^0
10^-1
0
1
10
100
1000

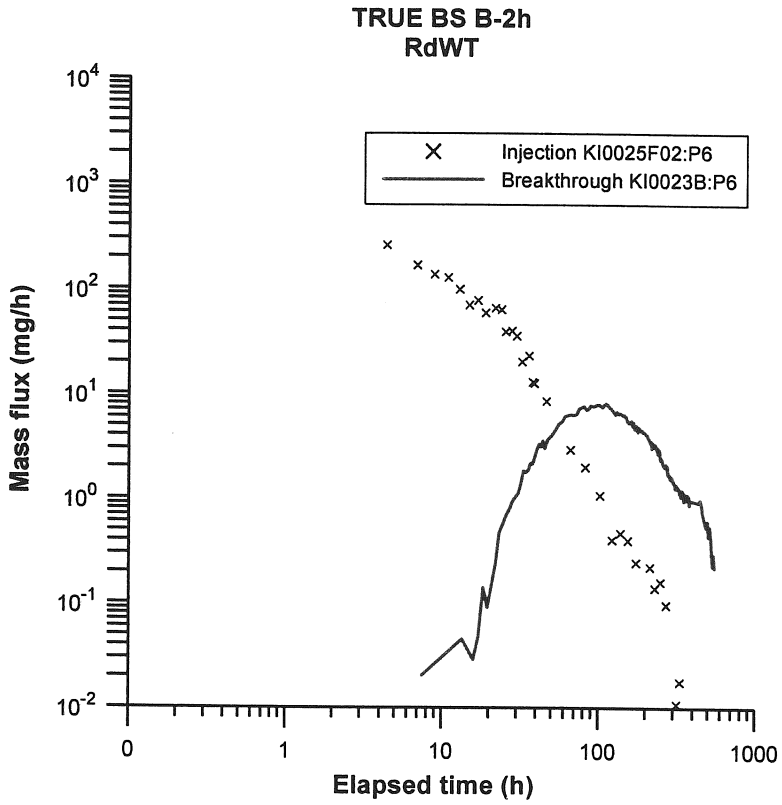
TRUE BS B-2h
RdWT
Injection KI0025F02:P6
Breakthrough KI0023B:P6
Mass flux (mg/h)
10^4
10^3
10^2
10^1
10^0
10^{-1}
10^{-2}
0
1
10
100
1000
Elapsed time (h)